MIT Libraries | DSpace@MIT

MIT Open Access Articles

Progress on ion cyclotron range of frequencies heating physics and technology in support of the International Tokamak Experimental Reactor

Massachusetts Institute of Technology

.

Progress on ion cyclotron range of frequencies (ICRF) heating physics and technology in support of the International Tokamak Experimental Reactor (ITER)

J.R. Wilson[1] and P.T. Bonoli[2]

[1]*Princeton Plasma Physics Laboratory PO Box 453, Princeton Jew Jersey 08543*

USA

[2]*Massachusetts Institute of Technology Plasma Science and Fusion Center,*

Cambridge, Massachusetts 02139, USA

Abstract

Ion cyclotron range of frequency (ICRF) heating is foreseen as an integral component of the initial ITER operation. The status of ICRF preparations for ITER and supporting research were updated in the 2007 [Gormezano 2007] report on the ITER physics basis. In this report we summarize progress made toward the successful application of ICRF power on ITER since that time. Significant advances have been made in support of the technical design by development of new techniques for arc protection, new algorithms for tuning and matching, carrying out experimental tests of more ITER like antennas and demonstration on mockups that the design assumptions are correct. In addition, new applications of the ICRF system, beyond just bulk heating, have been proposed and explored.

I.   Introduction

Ion cyclotron range of frequencies (ICRF) heating of tokamak plasmas has a long history of successful application. The principal technique of minority ICRF was pointed out by Stix [Stix 1975] and Perkins [Perkins 1977] and demonstrated on the ST, PLT and TFR tokamaks. Successful heating of DT plasmas was demonstrated on TFTR and JET [Wilson et al. 1995, Start et al. 1999, Phillips et al. 1999, Rimini et al. 1999]. The absorption schemes used there have formed the basis for the application of ICRF to ITER. New opportunities for utilization of the ICRF system, such as wall cleaning and flow drive have also been suggested and explored. Despite the success of ICRF heating, a number of issues remain to be solved to perfect the technique, such as the unwanted increase in impurity content of the plasmas during the heating. Additionally, as the desired power levels increase and the antenna structures become more sophisticated a wide variety of technical challenges need to be addressed. Many of these were summarized in the previous ITER physics data base review of 2007 [Gormezano et al. 2007]. In the sections below we will review progress made in this area since 2007.

II.   The basic role of ICRF on ITER

The principle use of ICRF on ITER will be to provide ion heating. ICRF has a long history of successful heating of tokamak plasmas both via the minority fundamental cyclotron absorption and via second harmonic damping. On ITER

the frequency capability of the system has been chosen to allow both of these mechanisms to be applicable in helium majority, deuterium majority and deuterium-tritium plasmas via hydrogen or helium-3 minority and tritium second harmonic damping at either full or half value of the toroidal magnetic field. In pure hydrogen plasmas only electron heating via Landau damping and transit time magnetic pumping would be available. Additional proposed uses of the ICRF system have arisen since the original ITER proposal. These include: Wall cleaning (ICWC), sawtooth control, central density and impurity control, and rotation drive.

III.   Description of the ITER ICRF system

The ICRF ITER system (see Fig. 1) (Lamalle et al. 2009) is envisioned to couple as much as 40 MW of RF power at frequencies between 40-55 MHz (Beaumont 2009). It presently includes two antennas mounted in mid-plane ports (Borthwick et al. 2009). Each antenna is expected to couple 20 MW to the plasma assuming a maximum antenna voltage of 45 kV. The exact amount delivered will of course depend on the coupling of the antenna to the plasma. Progress on modeling this will be discussed below. Unlike most present day ICRF antennas, which have a small number of radiating elements, each ITER antenna will have a complex array of 6 poloidal by 4 toroidal short length radiating straps (Fig. 2). They will be connected in 8 poloidal triplets fed from four transmitter units through a power splitting, phasing and pre-tuning transmission circuit. This arrangement, significantly more complicated than present day circuits, will present challenges

to the tuning and matching circuitry and software algorithms, which will be described in the following. The eight transmitters [Kazarian et al. 2011] are rated for 2.5 MW CW at a VSWR of 2 and 3MW at a VSWR of 1.5. Provision is made for increased power in an upgrade.

IV.   Technical Developments

Antenna Modeling and ITER like antenna performance

Predicting the performance of the ITER antenna is one of the real challenges in being able to guarantee system performance. Calculations of the antenna electromagnetic fields in the presence of plasma are necessary for obtaining the launched wave spectrum, the antenna voltage for a given power delivered and estimating parasitic fields which may lead to rectified sheaths and impurity production. Great strides have been made in 3D electromagnetic modeling at radio frequencies of detailed antenna structures using codes such as TOPICA [Milanesio et al. 2009], CST Microwave Studio® [Louche et al. 2011] and ANTITER II [Messiaen et al. 2010]. Increases in computer power and the development of new codes allowing for a more realistic plasma model have allowed calculation of complete antenna structures. These calculations have then been applied directly to the proposed ITER antenna designs [Messiaen et al. 2011, Milansio et al. 2010] Comparisons of code predictions with

experimental data from tokamaks [Argouarch et al. 2009] and from mock-ups [Kyrytsya et al. 2011] have been made with good agreement being found.

Starting with the ITER antenna design of 2007, an optimization of the design was performed [Milanesio et al. 2010]. In this study, using the TOPICA code with plasma, a 40% improvement in the power delivered at a fixed maximum antenna voltage could be achieved with geometrical modification of the transition from the radiating straps to the feeding coax (smoothing the transition) and of the horizontal septa (reducing the height) between the poloidal elements. In this study, as in others noted below it was found that, not surprisingly, increasing the vacuum gap between antenna and plasma strongly reduced the delivered power. Another analysis done with the commercial CST Microwave Studio® code [Louche et al. 2011] explored optimization of the antenna design by varying the strap width, depth of box and the four port junction (between the three poloidal radiating elements and the feed line). Additionally, the need for toroidal and poloidal alignment of the antenna was explored. Originally the design had a linear toroidal geometry, tangent to the plasma boundary surface. This led to uneven loading toroidally of the antenna straps. It was found that incorporating a simple two segment V-shape of the antenna in the toroidal plane was enough to obtain nearly uniform loading of the antenna elements.

The coupling between rf energy on the antenna and propagating waves in the core plasma is dominated by the edge plasma characteristics. A greater appreciation for the role of density gradients and the presence of a finite density SOL plasma in combination with newer antenna geometry has encouraged a more sophisticated approach to coupling calculations. It has been found [Messiaen et al. 2011] that three main parameters affect the coupling from the antenna to the plasma (Fig. 3). The first parameter is the long understood distance between the radiating elements and the radius where the plasma density equals the cut-off density for fast wave propagation. It has also been found that the amount of plasma in the region of density less than the cut-off density is not a strong factor. The second parameter is the position of an "optimal" density (which is greater than the cut-off density) with respect to the cutoff one. And the third parameter is the magnitude of the density gradient leading from the location of the optimal density to the plasma bulk. An important result of this analysis is that for the same antenna-cutoff distance, slight profile modifications can lead to substantial coupling and hence power handling variation. In addition to these constraints on the edge plasma parameters it was also found that proper toroidal and poloidal phasing is required to achieve the performance goal of 20 MW at 45 kV maximum voltage across the

entire frequency range. Wave numbers with $k_y > 0$ but near zero were found to be optimal. Monopole phasing had the highest loading but couples power to coaxial waves in the SOL. The incorporation of a service stub as part of the antenna structure was found to be necessary to broaden the frequency range.

Benchmarking of the code predictions with models of portions of the antenna has been performed [Argouarch et al. 2009, Kyrytsa et al. 2011]. TOPICA predictions were found to agree with a proto type of the older original ITER design [Agouarch et al. 2009] while CST Microwave Studio® predictions of the S parameters for one triplet of the newer design were found to be in excellent agreement with the measurements.

An "ITER like" antenna having eight radiating elements, similar to the original ITER design, and utilizing internal variable capacitors was installed and operated on the JET tokamak [Durodie et al. 2009, Durodie et al. 2012]. Bench testing of the antenna prior to installation allowed for evaluation of the matching algorithm designed to tune all four circuits simultaneously (Fig. 4). This was successfully demonstrated, although for a narrower frequency band, 47-49 MHz, than originally targeted. Commissioning of the antenna on JET plasmas was accomplished with rf power densities well in excess (>3x) of those achieved with the previously installed A2

antennas. The coupling results for L-mode plasmas agreed with the
TOPICA modeling. Operation at 42 kV was easily achieved boding
well for ITER's 45 kV requirement. The JET results confirmed the
advantages of using the conjugate-T system to achieve ELM
tolerance. The use of closely packed short straps to achieve high
power density did not pose any unforeseen problems in antenna
operation. Additionally, the high rf power density achieved did not
result in any increased impurity content or extra power deposited in
the SOL. This antenna also allowed the commissioning of the
SMAD (see below) arc protection system suitable for application on
ITER.

Matching

The ITER antenna will consist of a significantly larger number of
active elements than any existing antenna. Reliability will be a major
concern. Minimizing reflected power while controlling the antenna
spectrum in the presence of changing plasma loads, such as those
caused by ELM's or the L-H transition will be crucial to successful,
reliable application of ICRF heating on ITER. ICRF antennas
present a mismatched load (due to the low intrinsic wave impedance
of the fast wave) to the feeding transmission line. Therefore, some
kind of matching structure is required. This structure also frequently
serves as a power splitting and phase adjusting structure as well. A

review of matching techniques can be found in [Dumortier et al. 2010]. A desirable feature of such a structure would be to isolate the fluctuations in load due to ELM's (ELM resilience) from the transmitters. The baseline matching circuit for the ITER design utilizes hybrid couplers [Messiaen et al. 2009] to achieve ELM resilience. It was found that the mutual coupling between the triplets counteracted the load resilience and the spectrum control. Recall that increased mutual coupling was found to be necessary to achieve the operating voltage requirement. Matching solutions were designed that overcame these challenges. It was found that the array current spectrum can be controlled by feeding back on the phase of the anti-node voltage and, with suitable de-coupler circuits, the adverse effect of the mutual coupling can be neutralized. The conjugate-T matching solution is considered as a back-up option. An implementation of the hybrid coupler solution and its ability to couple power on ELM'y discharges was demonstrated on JET (Fig. 5) [Graham et al. 2012]. By utilizing different configurations on the various JET antennas comparisons were made with conjugate-T and internal matching layouts. These results supported the selection of the baseline hybrid design. A low power scaled mock-up of the ITER scheme was constructed and the tuning algorithms tested [Grine et al. 2012]. These measurements demonstrated an automatic feedback system

and algorithm able to track load variations while also being resilient to fast transients.

Other alternative matching techniques are being explored. These include dynamical matching involving variable capacitors and small variations in frequency [Prechtl et al.2009], the use of twin stubs and variable frequency [Kumazawa et al. 2008] and the use of fast ferrite tuners [Chen et al. 2012, Lin et al. 2009]. These methods, while involving the complication of adding active components, holds the promise of an ability to respond in real time to fast transients.

Arc Protection

An important element of the ICRF control system is arc protection. Electrical breakdown can occur in many places throughout the ICRF antenna, matching and transmission system. It can be due to the presence of high voltages between components, imperfections in the metal surfaces leading to electrical stress concentrations or to poor series connections that lead to over heating. Such breakdowns can lead to damage to the structures due to local energy deposition and injection of unwanted impurities into the plasma. In order to prevent this, the system must be able to quickly sense the presence of an arc and remove the rf power, which sustains the arc. Complicating the situation is that sudden changes in the plasma characteristics, such as

the L-H transition and ELM's, can mimic an arc in their effect on the antenna system.

An excellent summary of this issue for ITER is given by D'Inca [D'Inca et al. 2011]. Measuring the rf voltage reflection coefficient in the feed-lines near the transmitter outputs where, under matched load conditions, this ratio is small has traditionally been used to perform arc protection. Changes in the antenna load such as those due to an arc will mismatch the antenna leading to an abrupt increase in this signal. As noted above, other plasma effects can mimic this and series arcs (arcs in the conduction path) will not necessarily result in a significant change in this signal. In ITER, because the antenna consists of numerous radiating elements fed in parallel, the feed line impedance can be insensitive to a single arc depending on its location. Additionally, since the matching system for ITER is purposefully designed to minimize the effect of ELM's or the L-H transition on the reflection coefficient a collateral effect of desensitizing the system to arcs ensues. Due to these factors a number of alternative techniques for arc detection have been proposed and tested at various facilities.

A theoretical study for a Resonant Double Loop (RDL) antenna system demonstrated the utility of measuring the phases of the reflected rf signals [El Khaldibeen et al. 2010], a method that

proved valuable on the Alcator C-Mod tokamak and has been extended to ITER [Huygen et al. 2011].

During an arc, a plasma is formed and sustained by the arc energy. The discharge will have the usual plasma sheaths at the metal surfaces and hence will provide a non-linear impedance to the arc current. As a result of this non-linearity a spectrum of harmonics and noise will be created. Systems have been designed to detect either the harmonics or the sub-harmonic noise. The later has proven to be preferable due to the possible presence of pre existing harmonic content in the rf signals due to nonlinearities in the transmitter. Sub-Harmonic Arc Protection (SHAD) has been implemented on a number of tokamaks in a trial fashion. [Braun et al. 1996 Berger-By et al. 2007] Usually a band pass filter is applied to a sample of the rf power in the system. The filter removes very low frequency noise that can be induced by plasma fluctuations and has an upper cut-off below the applied rf frequency. One difficulty with this technique can arise if series capacitive elements are present in the antenna. These can present a high impedance to low frequency signals, isolating parts of the circuit, and prevent them from reaching the location that is being sampled. Spurious signals from other effects have also been observed in its implementation on JET [Jacquet et al. 2011].

Detecting arcs by optical means is often suggested. This technique has different requirements depending on whether it is implemented on the plasma side of the vacuum feed-through or the airside. The light emission characteristics of arcs have been studied in an attempt to find signals that can discriminate against plasma light [Dumortier et al. 2011]. They studied the time evolution of the light emission and the possibility of using line emission from ionized metal to discriminate arc light from plasma light. The ITER Like Antenna (ILA) used on JET provided a good test bed for ITER solutions. In addition to studying the SHAD concept [Jacquet et al. 2009] JET implemented a Scattering Matrix Arc Detection System (SMAD). The theory behind such a system was given in Vrancken [Vrancken et al. 2009]. The concept involves real time monitoring of the scattering matrix of the array and looking for changes in the relation between the elements of the matrix indicative of a change in the circuit parameters due to an arc. The performance of such a system in detecting arcs in the region of the T-junction of the JET ILA (a region of the circuit at low impedance where it is difficult to detect arcs with traditional methods) and its use in conjunction with a SHAD and reflection coefficient system is given in [Vrancken et al. 2011]. It was found to be effective at protecting against this type of fault.

An additional technique that has been utilized is audio detection.

Each of these techniques has its strengths and weaknesses, including

locations in the circuit where they are effective and others where

they are less thus a composite of these techniques may be required to

protect the antenna from all postulated faults with 100% reliability.

Such a system would add significant complication.

Localization of the arc location is important for repair purposes,

especially in a system like ITER's where the time to dismantle the

apparatus to look for arc damage would be prohibitive. A method

being explored for this purpose is the use of GUIDAR [Salvador et

al. 2011]. This method injects short phase modulated high frequency

pulses into the transmission line and looks for changes in the "echo"

pattern that can result from an arc and therefore from the timing of

the return allow a location to be determined.

V.   **Developments in the Physics of ICRF**

Basic theory

While the underlying physics of rf wave propagation and absorption have

been known for a long time, the ability to calculate the solutions to this

problem for realistic plasma geometries and parameters has continued to

evolve, especially with the continual increases in computational power.

Issues to be addressed include allowing for non-Maxwellian species, finite

orbit widths for particles, self-consistency between the non-thermal

particle distributions and the wave fields, inclusion of the full magnetic geometry, the presence of a separatrix and SOL plasma, and absorption at all cyclotron harmonics. An overview of the various numerical techniques used in calculating heating and current drive has been given by Van Eester. [Van Eester 2010]. An extension of the standard 1D Fokker-Planck modeling to arbitrary cyclotron harmonic and allowing for relaxation on non-Maxwellian species, including minority ion, majority ion, and electrons has been performed allowing for a quick assessment of competing heating schemes [Van Eester et al. 2011]. One approach to handling the problem of finite orbit widths and anisotropic equilibria is to utilize a suite of codes that evolved the equilibrium, wave fields and hot particle distributions separately until a self-consistent solution is found [Jucker et al. 2011]. This approach also allows an evaluation of the hot particle pinch. Recent work to add finite orbit width effects to a continuum Fokker Planck code have yielded much improved agreement between simulated and measured fast ion populations [Petrov et al. 2012]. Other approaches to calculating wave heating include coupling a Monte-Carlo code to the full wave linear absorption model instead of utilizing the Fokker-Planck approach [Choi et al. 2009] and the use of a variational approach to wave propagation and absorption [Dumont 2009]. The Monte-Carlo approach has the advantage that the typical methods used in calculation of the ion distribution functions due to neutral beam injection utilize this method and have been developed to a high degree. The

variational approach provides a common framework for the wave field calculation and the quasi-linear response of the particle distributions. This explicitly reveals the power transferred from the wave to the particles ensuring proper energy accounting even after approximations are made to simplify the solution for specific cases.

Heating Simulations

As both rf propagation and absorption codes and plasma transport codes have evolved in sophistication, simulation of the response of the ITER plasma to ICRF heating has become a major endeavor. A large number of studies have been carried out to assess whether the heating power mix between NNBI, ECH and ICRF as proposed for ITER operations is satisfactory [Parail et al. 2009, Budny 2009, Garcia et al. 2008, Wagner et al. 2010, Murakami et al. 2011, Citrin et al. 2010]. These studies typically included integrated transport, equilibrium and heating models. Study of the current ramp-up phase [Parail et al. 2009] verified that the required target q profiles for the H-mode, Hybrid and Steady State operation should be achievable with the present mix of NBI, ICRF and ECH. In a study of the full evolution of the baseline H-mode case [Budny 2009], wide variations in the core temperatures were seen during the current ramp with different heating mixes but the flat-top profiles were found to be very similar if the profiles are not too close to marginal stability values. The predicted toroidal rotation was found to be slow

(assuming $\chi_\phi//\chi_i$ =0.5) and only a little flow shear is present. The rotation

predicted by the GLF23 model [Waltz 1997] is greater by a factor of six

and significant flow shear would be present. The characteristics of the

pedestal, including edge temperature gradient are found to be more

important than the mix in achieving the Q=10 goal [Wagner et al. 2010].

The hybrid scenario adds the requirement of a more precise tailoring of the

current profile while still desiring Q $\geq$5. Since current drive is a more

power intensive requirement than heating it was found that a combination

of NBI and ECH was optimal [Citrin et al. 2010]. For steady state fully

non-inductive operation an internal transport barrier is required to achieve

a large enough bootstrap fraction to sustain the plasma current with the

envisioned auxiliary powers and desired Q [Garcia et al. 2008]. This

would require negative magnetic shear at an optimal location. It has

proven difficult to find a solution utilizing the proposed ITER heating mix.

[Wagner et al. 2010, Murakami et al. 2011, Poli et al. 2013] An alternative

solution for this scenario involving only rf has been presented. [Garcia et

al. 2008] This scenario employs ICRF, ECH and LH systems, utilizing the

ECH in particular to localize the minimum q value.

Benchmarking of the various codes used to predict ICRF

performance in the integrated modeling exercise has also been carried out

[Budny et al. 2012]. For the high performance baseline Q=10 plasma the

various full-wave codes were found to be in good agreement. For second

harmonic ^{3}He minority heating in hydrogen majority plasmas at half field

factors of two disagreements in the power absorption partition between species was found between the various codes.

New codes continue to be developed and applied to ITER predictions. The EVE code [Dumont 2009] derived from the variational approach used in conjunction with a Fokker-Planck solver was applied to the ITER DT case. [Dumont et al. 2013] The authors also point out the utility of applying simple 1D codes with radiative boundary conditions to estimate the single pass damping. For cases of low single pass absorption, full-wave codes usually exhibit eigenmode or cavity resonator behavior in the fields since edge losses are not typically included in the modeling. The AORSA code [Jaeger et al. 2001] was used for 3D calculations of the wave propagation and absorption in ITER relevant parameters. [Jaeger et al. 2008] These calculations [Jaeger et al. 2006] allowed for multiple ion species including impurities as well as non-Maxwellian ion distribution functions calculated by iterating the CQL3D Fokker-Planck code [Harvey et al. 1992] with full-wave solver AORSA.

Experimental results

Experiments continue to be performed on existing devices that are designed to elucidate details of what can be expected in various regimes on ITER as well as supporting additional applications of ICRH in tokamaks. Of special interest have been experiments on H-mode plasmas

evaluating various combinations of the heating sources as envisioned on ITER and experiments evaluating plasma rotation during ICRF heating. Comparisons of H-mode behavior for various heating methods were studied on both JET [Versloot et al. 2011] and ASDEX-Upgrade (Fig. 6) [Sommer et al. 2011]. Studies of high non-inductive current fraction H-modes were performed on NSTX [Taylor et al. 2012]. In the JET experiment a comparison of dominant NBI and dominant ICRF heated ELMy H-mode plasmas was performed. No significant differences in the density and temperature profiles or global confinement were found. Some small variations in the ion temperature profiles could be obtained by varying the deposition profile. Also, overall changes in H-mode performance due to changes in the plasma density and/or power levels were independent of the heating mix. On ASDEX-U combinations of NBI, ICRF and ECH were explored in order to investigate the performance results due to the competition between electron and ion heating. The role of NBI and ICRF (both of which heat a mixture of electrons and ions) were found to be similar. Some variation in the ELM characteristics were seen as the power mix varied but the overall H-mode performance did not. It should be noted that even in a nearly pure electron heating case the high collisionality ASDEX-U discharges remain in the ITG dominated transport regime. The purely ICRF driven H-modes at high non-inductive current fraction (0.7-1.0) on NSTX featured internal transport barriers with large values of T_e/T_i.

Plasma rotation has been found to be an important parameter for plasma stability and confinement. While rotation in present day experiments tends to be dominated by the external torque applied, in ITER this will not be the case and the intrinsic rotation of the plasma will dominate. Rotation driven by mode conversion flow drive will be discussed below. In JET experiments [Eriksson et al. 2009] the plasma rotation resulting from standard minority heating was investigated. Antennas were phased such that direct injected momentum was small. The edge region was found to rotate in the co-current direction for all cases with the velocity scaling as stored energy divided by electron density. The torque driving this rotation appears to be at the edge and unrelated to the presence of fast ions. The central rotation profile could vary from slightly peaked to hollow depending on plasma parameters. A scaling depending on plasma current divided by electron density could be inferred from the data. It was suggested that at low values of the plasma current, the hollow profiles might be driven by a torque from the fast ion population. In other experiments [Hellsten et al. 2012], dominant electron heated scenarios were studied. Central counter current rotation was observed, scaling with the electron temperature indicating that changes in electron transport may be driving the rotation effects.

Randy – should we add results here about the toroidal rotation results observed in C-Mod with balanced ICRF injection ?? That would be say from one of the papers by Rice – or do you think these results are too old ?

Detailed measurements of the fast ion population during ICRF were made in Alcator C-Mod and NSTX [Bader et al. 2012, Tang et al. 2007, Liu et al. 2010]. On NSTX, calculations with a zero banana width Fokker-Planck code were not found to be in agreement for combined NBI and high harmonic ICRF. This may be due to the zero banana width assumption (banana widths are quite large in NSTX). A further possible cause was the observed increase in Compressional Alfven Wave mode activity during the combined heating. On Alcator C-Mod the fast proton (D-H minority heating) distribution was peaked off axis even when the resonance was on axis. This was ascribed to a combination of poor wave focusing in the small Alcator C-Mod plasma and to the high rf power density leading to a large trapped ion population. Measurements were made up to 2 MeV. An unusual feature in C-Mod is a strong dependence of the tail temperature on plasma current and a saturation in the temperature at high powers (> 2MW). These effects were also postulated to be a consequence of the high rf power density in Alcator C-Mod ICRF experiments.

Heating modes

Basic application of ICRF on ITER will involve second harmonic tritium heating with, perhaps, the addition of a small amount of ^{3}He minority. This regime was previously demonstrated on TFTR [Wilson et al. 1995, Phillips et al. 1999] and JET [Start et al. 1999, Rimini et al. 1999] and should provide a robust heating method for the DT phase at full magnetic

field. A variety of other, more exotic, heating regimes have been proposed for both the pre-DT phase, for operation at reduced toroidal field values and as back-up scenarios for the full DT phase. Several of these have been tested on existing devices. Of particular concern is the demonstration of viable heating schemes for the pre deuterium phase of ITER operation given the frequency constraints of the ITER ICRF system. At full magnetic field with ^{4}He as the working gas either hydrogen or ^{3}He minority heating could be used. If hydrogen is the working gas then ^{3}He minority heating could be used. An alternative to minority heating would be to heat the majority ion at its fundamental resonance. In a cold single ion species plasma there is no absorption of the fast wave at the fundamental resonance due to the wave polarization at resonance being counter to the ion gyro motion. In hot plasmas the resonance is Doppler broadened and absorption can occur. Pure fundamental damping has been explored in experiments on JET (Fig. 7) [Krasilnikov et al. 2009] and through modeling of those experiments [Lerche et al. 2009]. In these experiments it was found that absorption in the ohmic target plasma was too weak to allow effective heating but in the presence of energetic NBI ions Doppler broadened absorption produced significant increases in the electron and ion temperatures. A surprising result was that heating was more effective with 80 keV beam injected ions than with 130 keV injected beam ions. With the weak absorption observed in these JET experiments enhanced impurity injection and an increase in Z_{eff} took place when the rf

power was switched on. Modeling of these experiments [Lerche et al. 2009] found agreement with the power absorption profiles determined from break-in-slope analysis of electron cyclotron emission (ECE) and charge exchange signals supporting the basic absorption mechanism. The authors point out that fundamental minority absorption on or near deuterium like impurity species (such as Be^9) can be expected to occur if the fundamental resonance is in the plasma. In another analysis, [Kazakov et al. 2012] the consequences of varying the D to T ratio achieving a transition from cyclotron damping to mode conversion heating was explored. It was found that a roughly 50-50 ratio actually suffered from parasitic absorption on fusion alphas and NBI fast ions. Taking advantage of a constructive interference effect between transmitted and reflected waves in the mode conversion region [Fuchs et al. 1995] it was found that the optimum concentration would be 80% T and 20% D with a heating efficiency comparable to the standard ^{3}He minority in 50:50 DT plasma (Fig. 8). Looking at the other end of the concentration spectrum tritium minority heating has been suggested [Castaldo et al. 2010] as a means of producing increased reactivity by generating a non-Maxwellian tritium tail. The authors examined second harmonic tritium damping of a mode converted Ion Bernstein wave. They estimate that for JET a Q value in excess of unity could be obtained in a plasma consisting of 75% deuterium and 25% tritium. Mode conversion heating has been studied on JET in ^{3}He-H plasmas [Van Eester et al. 2012, Kiptily et al. 2012]. The ^{3}He

concentration, η, was varied from 0-25%. Three regimes of heating were observed. For concentrations less than 1.8% minority heating was observed with ^{3}He ions accelerated into the MeV range. For $\eta > 6\%$ mode conversion heating was seen. For $1.8\% < \eta < 5\%$ a mixture of minority and mode conversion heating was found. Mode conversion heating was seen to be as effective as minority heating. A difficulty in these experiments, that would not be expected to occur in ITER (for the pre deuterium phase), is the complication added by having a small amount of deuterium present (sourced from the walls etc. from previous experiments). This makes operation at 5-6% ^{3}He difficult because an additional mode conversion and evanescent zone appears right in front of the antenna preventing effective wave coupling to the core plasma. Concentration scans were also carried out for the more conventional ^{3}He-D plasmas in JET [Van Eester et al. 2009] where a similar separation into minority heating, mode conversion and a mixed scenario was documented. For operation at half values of the magnetic field, expected to be required early on in ITER operation, further difficulties arise. The only available minority scheme would be second harmonic ^{3}He. The other proposed scheme would be fundamental H majority. Both of these schemes were investigated on JET [Lerche et al. 2012]. Given the lower target temperature in JET than that expected in ITER it isn't surprising that these schemes were plagued by weak absorption, $P_{abs}/P_{launched} < 40\%$. The results indicated dominate electron heating accompanied by enhanced

plasma-wall interaction as exemplified by high radiation losses and increased impurity content. The latter effect was stronger in the ^{3}He case and effective heating was only observed for concentrations >20%. Some improvement in the H case was seen with increasing target temperature, whereas the important variable for the minority case was minority concentration. An alternative ICRF heating scheme that is now being considered for ITER half-field operation is the use of a majority He plasma with a H minority component. This would be expected to have the same strong single pass absorption as the D (H) minority heating scheme. The only concern for this application would be the limit on H concentration so as not to negatively impact the power threshold for L to H transition.

Edge/SOL

Increasingly, it has been understood that the behavior of the interaction between the ICRF antennas and the scrape-off layer (SOL) plasma is of crucial importance in determining the overall performance of ICRF in a tokamak. Much of the deleterious behavior, production of impurities, density increase etc., has been ascribed to the generation of rf sheath potentials on various bounding materials. A large effort has gone into understanding how these sheaths are formed and how the can be

minimized [Myra et al. 2008, Kohno et al. 2012, D'Ippolito et al. 2009, D'Ippolito et al. 2008, D'Ippolito et al. 2010, Myra et al. 2009, Mendes et al. 2010]. In a series of papers Myra and D'Ippolito have outlined the physics of the rf induced sheaths and how to apply this to the boundary condition imposed in 3D electromagnetic codes that are used to calculate the rf fields near the antenna and in the SOL. They have pointed out the role played by the slow wave [Myra et al. 2008,2009] in both tenuous and over dense plasmas. This includes the possibility that the sheath boundary condition allows for the localized excitation of slow (LH like) waves. Strong amplification of the induced sheath potential can occur for close in limiters due to a sheath-plasma resonance. Additionally, the role of far-field sheaths has been investigated [D'Ippolito et al. 2008]. These sheaths occur when unabsorbed rf wave energy, due either to weak single pass damping through the core plasma or to waves propagating in the SOL, encounters a conducting surface that is not aligned with a flux surface. Similar to the near field sheaths a sheath-plasma-wave resonance can occur amplifying the sheath potential.

Predictions of the sheath theory were tested on Tore-Supra [Mendes et al. 2009]. Their results supported the role of parallel (to the magnetic field) flowing currents on antenna structures in driving the sheath potentials that resulted in antenna hot spots. They proposed two methods to reduce these currents. The first, applicable to many present-day antennas that protrude from the tokamak wall, is to slot the horizontal structures (impeding

parallel current flow) and avoid closed current paths on the Faraday shield. The second, applicable to antennas, like ITER's, that are recessed behind the first wall, consists of cancelling as much parallel current as possible by achieving better alignment with the magnetic field by tilting the antenna structure.

The tilted antenna approach is best exemplified on the Alcator C-Mod device (Fig. 9) [Garrett et al. 2011,Wukitch et al. 2013] where a completely helically aligned design was implemented. While a marked reduction in impurity production and plasma impurity concentration was achieved, the measured rf potentials in the SOL were not affected (Fig. 10). This would indicate that a significant fraction of the impurity production is not a function of the magnitude of the rf electric field parallel to the magnetic field. An additional benefit of this design was an increase in the voltage handling and an improvement in performance at high values of plasma and neutral density.

In addition to sheath formation ICRF can interact with the SOL plasma in a variety of ways. Large scale turbulent structures (so called "blobs") in the SOL can be suppressed during ICRF [Antar et al. 2010, 2012]. ELM induced transport could also be reduced. The effect showed no scaling with power although a low power threshold could not be ruled out. The effect was observed close to the antennas but not necessarily on field line connected surfaces. In NSTX wave power flowing in the SOL was observed to link to hot spots in the divertor region [Perkins et al. 2012].

This flow was also seen to involve field lines that did not connect directly to the antennas, but originated between the antenna structure and the last closed flux surface in the SOL. Acceleration of ions was seen in the SOL on DIII-D [Pace et al. 2012]. Ions with energies greater than 20 keV originating in the SOL were observed on loss probes. It is believed that parametric decay into ion Bernstein waves that are then absorbed at high harmonics in the SOL are responsible for the ion acceleration. The structure of the radial electric field in the SOL due to the excitation of the ICRF antenna has been explored on Alcator C-Mod [Cziegler et al. 2012]. Gas puff imaging techniques are employed to look for poloidal flows due to radial electric fields. The field is seen to extend into the SOL and have a magnitude of 20-30 kV/m. The plasma potential is found to scale as $P_{rf}^{0.5}$ and is peaked near the top and bottom of the antenna consistent with sheath rectification. The radial penetration is found to be much larger than the skin depth.

Density modification of the SOL plasma is also common [Kirov et al. 2009, Van Eester et al. 2013]. On JET, a degradation in coupling between the lower hybrid current drive launcher and the plasma during ICRF has been ascribed to a strong reduction in the plasma density along field lines connected to the ICRF antennas [Kirov et al. 2009]. This density loss can be ameliorated by gas puffing to replace the lost density. This effect has been ascribed to the poloidal gradients in the rf field giving rise to radial

density motion and to the radial gradients yielding poloidal asymmetries [Van Eester et al. 2013].

Tungsten

Since ITER will have all metal plasma facing materials, several tokamaks have converted over to all metal components including tungsten ones. The generation of tungsten impurities in the edge plasma, especially from antenna protection elements, is a significant concern given the high atomic number of tungsten. The first ICRF experiments in a tokamak with an all tungsten wall have been conducted on ASDEX Upgrade [Bobkov et al. 2010]. Enhanced sputtering of tungsten was seen during ICRF heating. Reductions in the amount of tungsten sputtering could be achieved by: increasing the plasma-antenna distance (but this reduces the coupling), strong gas puffing [Jacquet et al. 2012], decreasing the light impurity content of the plasma [Sips et al. 2008] (light impurities cause more sputtering per ion than deuterium), or by reducing the antenna rf electric fields parallel to B. This latter can be accomplished by changes in the antenna box geometry, increasing the distance between straps and the box and by proper phase balance of the antenna currents.

Behavior of impurities in the core plasma

Transport of impurities in the main plasma can be altered by the
application of rf. This may be used to "flush" impurities out of important
regions of the plasma. Additionally, under intense minority heating, a
poloidal asymmetry in the high Z impurity concentration has been
observed in Alcator C-Mod [Reinke et al. 2012]. In-out asymmetries in the
molybdenum concentration of up to a factor of 2 were observed during H
minority heating. The ratio was found to depend on the major radius of the
minority ion cyclotron layer. The asymmetry was ascribed to the poloidal
variation in the plasma potential created by the presence of the fast
minority trapped ion population. A theoretical study of this effect
[Kazakov et al. 2012] resulted in the derivation of an approximate
expression for the asymmetry as a function of plasma parameters, ICRF
power and resonance location. It was found to depend strongly on the Z of
the impurities, increasing with Z. A calculation of the effect of the local
ponderomotive force on trace impurity transport was found to have a
minor effect on the steady state impurity concentration peaking factor
[Nordman et al. 2008}. A study on JET [Valisa et al. 2011] explored
changes in impurity transport in the presence of central ICRF heating.
Core pump-out of Ni and Mo were observed with central electron heating
at low collisionality. In the absence of ICRF, strong peaking of the
impurity profiles was observed and the inferred direction of impurity flow
was seen to reverse for rf power levels in excess of 3 MW. In another
study on JET [Czarnecka et al. 2012] the total core impurity content of Ni

was seen to vary with antenna phasing and the use of gas puffing to improve the antenna coupling. Impurity content was seen to be minimized by using those phasings and gas puffing techniques, including location of gas injection, which led to the best antenna coupling.

Additional Applications of ICRF possible on ITER

Mode conversion flow drive

Several additional, more exotic, applications of ICRF have been proposed and explored both experimentally and theoretically. One of these is the possibility to directly drive plasma flows locally from rf wave absorption. It has been observed experimentally that such flows can occur during mode conversion heating and current drive (Fig. 11). The theoretical foundation for explaining and predicting these flows is still under development. The theory of mode conversion was extended to multiple ion species [Kazakov et al. 2010] to look at the possibility of enhancements predicted earlier [Fuchs et al. 1995] taking into account the role of carbon impurity ions. It was seen that for JET parameters, enhanced mode conversion could be expected and may explain earlier experimental results. On Alcator C-Mod measurement of the mode converted waves in D-H and D-^{3}He plasmas were compared to theory [Tsuji et al. 2012]. It was found that the location and wavelength of the mode converted wave agreed with theory as well as the scaling with power

but the magnitude of the detected wave, while agreeing with the simulations at low levels of intensity was a factor of 50 too small at high levels of intensity. A number of experiments observed plasma flows associated with mode conversion [Lin et al. 2008, Lin et al. 2011, Lin et al. 2012, Zhang et al. 2012]. In these experiments radially localized flows in the poloidal direction were observed and more broadly the toroidal rotation profile was affected. The magnitude of observed rotation velocity changes were significantly larger than those observed for minority heating cases. The dependence on launched wave spectrum was consistent with mode conversion theory in that it was asymmetrical in toroidal wave number. The magnitude of the flow scaled with rf power and with plasma current and inversely with plasma density. In the JET experiments an optimum range of minority concentration, 10-17%, was found. Not all aspects of the C-Mod and JET experiments could be reconciled with each other indicating that further understanding of the underlying mechanism is required.

Sawtooth Control

A secondary but very valuable application of ICRF heating and/or current drive is sawtooth control. The presence of a significant energetic alpha particle population could lead to the presence of monster sawteeth in burning ITER plasmas. These sawtooth oscillations could provide the seed for Neoclassical Tearing Mode (NTM) destabilization or a large

redistribution of both the alphas and any other energetic ions before they can slow down. The use of ICRF to destabilize the sawtooth oscillation before it can grow to large amplitude has been demonstrated on a number of devices (Fig. 12) [Lennholm et al. 2011, Parisot et al. 2007, Graves et al. 2010]. Originally it was proposed that the stabilization was due to ICRF driven currents that modified the magnetic shear at the q=1 surface. A new explanation of the mechanism of stabilization due to radial drift excursion of energetic passing ions contributing to the stability of the mode was given by Graves [Graves et al. 2009]. This was further elaborated and accompanied by detailed numerical modeling in a paper by Chapman [Chapman et al. 2011]. By using ^{3}He minority ions the amount of current drive could be minimized supporting the argument that the presence of an asymmetric passing fast ion population affected the stability of the mode directly. [Graves et al. 2010, Graves et al. 2011]. Sawtooth destabilization on ITER by ICRF would be easier to accomplish if this mechanism continues to hold since it would require less power.

Wall Cleaning

Being able to "clean" the surfaces of materials exposed to the ITER plasma will be crucial both for optimized plasma performance and for Tritium inventory control. Conventional Glow discharge cleaning is hampered by the presence of the steady state toroidal field in ITER and other superconducting devices. Use of the ICRF system to produce a "wall

scrubbing" plasma has been developed on a number of tokamak devices. [Lyssoivan et al. 2012, Paul et al. 2012, Lee et al. 2011, Paul et al. 2013, Yu et al. 2011]. Advantages of this technique include ability to operate at the steady state magnetic field value of the machine so that the superconducting magnets can remain on and use of the already existing ICRF infrastructure without added components. Challenges to the technique include: How to fill the entire chamber with plasma, avoiding breakdown in the ICRF antennas, the ability of the technique to penetrate the divertor and between protective tiles. Figure 13 shows the successful operation of the JET A2 antennas for wall cleaning. Significant strides have been made in understanding the process even though a full first principles calculation of rf breakdown of the fill gas under these conditions is beyond the ability of existing codes. Achieving sufficient plasma loading of the antenna while still maintaining low neutral pressure was solved by three techniques. First, operating the antennas in monopole phasing producing a low $k_{\parallel}$ spectrum which has a lower plasma density required for fast wave propagation. Second, use of mode conversion from fast to slow to Ion Bernstein wave (IBW). This is possible in a two-ion species plasma. Or third, operation at high cyclotron harmonic number (this will not be possible for ITER unless the toroidal field is reduced) was found to also be effective. Spreading out of the plasma to fill the chamber was found to be aided by the addition of a small vertical magnetic field.

Summary

ICRF heating of the ITER plasma will play a crucial role in the success of ITER. Since the last review in 2007 significant advances in ICRF heating technology and physics understanding have taken place. The main application, heating of the plasma ions via the second harmonic tritium resonance is an established technique but new applications have been brought forward such as sawtooth control, rotation drive and wall cleaning. Alternate heating schemes and especially ones for the pre activation phase have been proposed and explored on existing devices. The ITER ICRF system will be the most complicated such system to date. Technical challenges arise from the unprecedented levels of rf power required to be coupled to the plasma, the long pulse lengths involved as well as the need for very high reliability and the difficulty of maintenance. The ITER antenna design contains a large number of coupled radiative elements necessitating new approaches to tuning, matching and arc protection. Calculation, as well as construction of prototypes and bench testing has confirmed many of the proposed ITER design elements, Additionally, experiments on existing devices have explored various approaches that could be applied to the ITER system. Much experimental and theoretical effort has been devoted to understanding the interaction between the ICRF antenna and the SOL plasma. The formation of rf driven sheaths and their effect on the boundary conditions used in calculating rf fields in the SOL have been extensively explored. New antenna designs, such as the Alcator C-Mod fully field aligned antenna have added to or understanding.

Acknowledgments

References

1. Antar, G.Y., Goniche, M., Ekedahl, A., and Colas, L. Nuclear Fusion 52 (2012) 103005.

2. Antar, G., Assas, S., Bobkov, V., Noterdaeme, J.-M., Wolfrum, E., Herrmann, A., Rohde, V., and ASDEX Upgrade Team, Physical Review Letters 105 (2010) 165001.

3. Argouarch, A., Vulliez, K., Mollard, P., Lombard, G., Bosia, G., Colas, L. Mendes, A., Volpe, D., Millon, L., Ekedahl, A., et al., Fusion Engineering and Design 84 (2009) p. 275.

4. Bader, A., Granetz, R.S., Parker, R.R., Bonoli, P.T., Hutchinson, I.H., Sears, J., and Wukitch, S.J., Nuclear Fusion 52 (2012) 094019.

5. Berger-By, G., Beaumont, B., Lombard, G., Millon, L., Mollard, P., and Volpe, D., Fusion Engineering and Design 82 (2007) p. 716.

6. Beaumont, B. 23rd Symposium on Fusion Technology 2009 doi: 10.1109/Fusion 2009.5226425.

7. Bobkov, Vl.V., Braun, F., Dux, R., Herrmann, A., Giannone, L., Kallenbach, A., Krivska, A., Muller, H.W., Neu, R., Noterdaemme, J.-M., et al., Nuclear Fusion 50 (2010) 035004.

8. Borthwick, A., Agarici, G., Davis, A., Dumortier, P., Durodie, F., Fanthome, J., Hamlyn-Harris, C., Hancock, A.D., Lockley, D., Mitteau, R., et al., Fusion Engineering and Design 84 (2009) p. 493.

9. Braun, F., and Sperger, Th., Proceedings of the 19th Symposium on Fusion Technology (1996) p. 601.

10. Budny, R.V., Nuclear Fusion 49 (2009) 085008.

11. Budny, R.V., Berry, L., Bilato, R., Bonoli, P., Brambilla, M., Dumont, R.J., Fukuyama, A., Harvey, R., Jaeger, E.F., Indireshkumar, K., et al., Nuclear Fusion 52 (2012) 023023.

12. Castaldo, C. and Cardinali, A., Physics of Plasmas 17 (2010) 072513.

13. Chapman, I.T., Graves, J.P., Johnson, T., Asunta, O., Bonoli, P., Choi, M., Jaeger, E.F., Jucker, M., and Sauter, O., Plasma Physics and Controlled Fusion 53 (2011) 124003.

14. Chen, G., Zhao, Y. Mao, Y., Yuan, S., Zheng, G., Zheng, F., He, Z., and Yu, S., Fusion Science and Technology 61 (2012) p. 301.

15. Choi, M., Chan, V.S., Berry, L.A., Jaeger, E.F., Green, D., Bonoli, P., Wright, J., and the RF SciDAC Team, Physics of Plasmas 16, (2009) 052513.

16. Citrin, J., Artaud, J.F., Garcia, J. Hogeweij, G.M.D., and Imbeaux, F., Nuclear Fusion 50 (2010) 115007.

17. Czarnecka, A., Durodie, F., Figueiredo, A.C.A., Lawson, K.D., Lerche, E., Mayoral, M.-L., Ongena, J., Van Eester, D., Zastrow, K.-D., Bobkov, V., et al., Plasma Physics and Controlled Fusion 54 (2012) 074013.

18. Cziegler, I., Terry, J.L., Wukitch, S.J., Garret, M.L., Lau, C., and Lin, Y., Plasma Physics and Controlled Fusion 54 (2012) 105019.

19. Dumont, R.J., Nuclear Fusion 49 (2009) 075033.

20. Dumortier, P., and Messiaen, A., Transactions on Fusion Science and Technology 57 (2010) p. 230.

21. Dumortier, P., Huijser, T., D-Inca, R., Faugel, H., Hangan, D., Huygen, S., Messiaen, A., Onyshchenko, A., Siegel, G., van der Valk, N.C.J., and Vervier, M., Fusion Engineering and Design 86 (2011) p 831.

22. Durodie, F., Nightingale, M.P.S., Mayoral, M-L., Ongena, J., Argouarch, A., Berger-By, G., Blackman, T., Cocilovo, V., Czarnecka, A., Dowson, S., et al., Plasma Physics and Controlled Fusion 54 (2012) 074012.

23. Durodie, F., Nightingale, M., Argourach, A., Berger-By, G., Blackman, T., Caughman, J., Cocilovo, V., Dumortier, P., Edwards, P., Fanthome, J., et al., Fusion Engineering and Design, 84 (2009) p. 279.

24. El Khaldi, M., Bosia, G. Vulliez, K., and Magne, R., Fusion Engineering and Design 85 (2010) p. 7.

25. Eriksson, L-G., Hellsten, T., Nave, M.F.F., Brzozowski, J., Holmstrom, K., Johnson, T., Ongena, J., Zawstrow, K.-D., and JET-EFDA Contributors, Plasma Physics and Controlled Fusion 51 (2009) 044008.

26. Fuchs, V., Ram, A.K., Schultz, S.D., Bers, A., and Lashmore-Davies, C.N., Physics of Plasmas 2 (1995) p. 1637.

27. Garcia, J., Giruzzi, G., Artaud, J.F., Basiuk, V., Decker, J., Imbeaux, F., Peysson, Y., and Schneider, M., Plasma Physics and Controlled Fusion 50 (2008) 124032.

28. Garrett, M.J., Wukitch, S.J., Koert, P., Whyte, D.G. Proceedings of the 19th Topical Conference on Radio Frequency Power in Plasmas, Newport, Rhode Island, USA, AIP Conference Proceedings, 1406 (2011) p. 203.

29. Gormezano, C. Sips, A.C.C., Luce, T.C., ide, S., Becoulet, A., Litaudon, X., Isayama, A., Hobrik, J., Wade, M.R., Oikawa, T., et al., Nuclear Fusion 47 (2007) S285.

30. Graham, M. Mayoral, M-L., Monakhov, I., Ongena, J., Blackman, T., Nightingale, M.P.S., Woolridge, E., Durodie, F., Argouarch, A., Berger-By, G., et al., Plasma Physics and Controlled Fusion 54 (2012) 074011.

31. Graves, J.P., Chapman, I., Coda, S., Eriksson, L.-G., and Johnson, T., Physical Review Letters 102 (2009) p. 06005-1.

32. Graves, J.P., Chapman, I., Coda, S., Johnson, T., Lennholm, M., Alper, B., de Baar, M., Crombe, K., Eriksson, L.-G., Felton, R., et al. Nuclear Fusion 50 (2010) 052002.

33. Graves, J.P., Chapman, I.T., Coda, S., Johnson, T., Lennholm, M., Paley, J.I., Sauter, O., and JET-EFDA Contributors, Fusion Science and Technology 59 (2011) p. 539.

34. Grine, D., Messiaen, A., Vervier, M., Dumortier, P., and Koch, R., Fusion Engineering and Design 87 (2012) p. 167.

35. Harvey, R. and McCoy, M.G., Proceedings of the IAEA Technical meeting on Simulation and Modeling of Thermonuclear Plasmas, Montreal Canada, 1992 (USDOC NTIS Document No. DE93002962).

36. Hellsten, T., Johnson, T.J., Van Eester, D., Lerche, E., Lin, Y., Mayoral, M.-L., Ongena, J., Calabro, G., Crombe, K., Frigone, D., et al., Plasma Physics and Controlled Fusion 54 (2012) 074007.

37. Huygen, S. Dumortier, P., Durodie, F., Messiaen, A., Vervier, M., Vrancken, M., Woolridge, E., and the CYCLE Team, Proceedings of the 19th Topical Conference on Radio Frequency Power in Plasmas, Newport, Rhode Island, USA, AIP Conference Proceedings, 1406 (2011) p. 21.

38. D'Inca, R., Proceedings of the 19th Topical Conference on Radio Frequency Power in Plasmas, Newport, Rhode Island, USA, AIP Conference Proceedings 1406 (2011) p. 5.

39. D'Ippolito, D.A. and Myra, J.R., Physics of Plasmas 16 (2009) 022506.

40. D'Ippolito, D.A. and Myra, J.R., Physics of Plasmas 17 (2010) 072508.

41. D'Ippolito, D.A., Myra, J.R., Jaeger, E.F. and Berry, L.A., Physics of Plasmas 15 (2008) 102501.

42. Jaeger, E.F., Harvey, R.W., Berry, L.A., Myra, J.R., Dumont, R.J., Phillips, C.K., Smithe, D.N., Barrett, R.F., Batchelor, D.B., Bonoli, P.T., et al., Physics of Plasmas **13**, 056101 (2006).

43. Jaeger, E.F., Berry, L.A., D'Azevado, E., Batchelor, D.B., and Carter, M.D., Physics of Plasmas 8 (2001) p. 1573.

44. Jaeger, E.F., Berry, L.A., D'Azevado, E., Barrett, R.F., Ahern, S.D., Swain, D.W., Batchelor, D.B., Harvey, R.W., Myra, J.R., D'Ippolito, D.A., et al., Physics of Plasmas 15 (2008) 072513.

45. Jacquet, P., Berger-By, G., Bobkov, V., Blackman, T., Durodie, F., Mayoral, M-L., Nightingale, M., and JET-EFDA Contributors, Proceedings of the 18th Topical Conference on Radio Frequency Power in Plasmas, Ghent, Belgium, AIP Conference Proceedings 1187 (2009) p 241.

46. Jacquet, P. Berger-By, G. Bobkov, V., Blackman, T., Day, I.E., Durodie, F., Graham, M., Hellsten, T., Laxaback, M., Mayoral, M.-L., et al. Proceedings of the 19th Topical Conference on Radio Frequency Power in Plasmas, Newport, Rhode Island, USA, AIP Conference Proceedings 1406 (2011) p. 17.

47. Jacquet, P., Bobkov, V., Mayoral, M-L., Monakhov, I, Noterdaeme, J.-M., Scarabosio, A., Stepanov, I.,Vranken, M., Wolfram, E. and the ASDEX Upgrade Team, Nuclear Fusion 52 (2012) 042002.

48. Jucker, M., Graves, J.P., Cooper, W.A., and Johnson, T., Plasma Physics and Controlled Fusion 53 (2011) 054010.

49. Kazakov., Y.O., Pavlenko, I.V., Van Eester, D., Weyssow, B., and Girka, I.O., Plasma Physics and Controlled Fusion 52 (2011) 115006.

50. Kazakov, Y.O., Kiptily, V.G., Sharapov, S.E., Van Eester, D., and JET-EFDA Contributors, Nuclear Fusion 52 (2012) 094012.

51. Kazakov, Y.O., Pusztai, I., Fulop, T. and Johnson T., Plasma Physics and Controlled Fusion 54 (2012) 105010.

52. Kazarian, F., Beaumont, B., Arambhadiya, B., Gassmann, T., Lamalle, P., Rathi, D., Mukherjee, A., Ajesh, P., Machchhar, H., Patadia, D., et al., Fusion Engineering and Design 86 (2011) p. 888.

53. Kiptily, V.G., Van Eester, D., Lerche, E., Hellsten, T., Ongena, J., Mayoral, M.-L., Cecil, F.E., Darrow, D., Gatu Johnson, M., Goloborod'ko, V., et al., Plasma Physics and Controlled Fusion 54 (2012) 074010.

54. Kirov, K.K., Mayoral, M-L., Mailloux, J., Baranov, Y., Colas, L., Ekedahl, A., Erents, K., Goniche, M., Korotkov, A., Morgan, P., et al., Plasma Physics and Controlled Fusion 51 (2009) 044003.

55. Kohno, H., Myra, J.R., and D'Ippolito, D.A., Physics of Plasmas 19 (2012) 012508.

56. Krasilnikov, A.V., Van Eester, D., Lerche, E., Ongena, J., Amosov, V.N., Biewer, T., Bonheure, G., Crombe, K., Ericsson, G., Esposito, B., et al., Plasma Physics and Controlled Fusion 51 (2009) 044005.

57. Kyrytsya, V., Dumortier, P., Louche, F., Messiaen, A. and Vervier, M., Fusion Engineering and Design 86 (2011) p, 901.

58. Kumazawa, R. Saito, K., Kasahara, H., Seki, T., Mutoh, T., Shimpo, F., Nomura, G., Kato, A., Okada, H., Zhao, Y., et al., Nuclear Fusion 48 (2008) 115002.

59. Lamalle, P.U., Beaumont, B., Gassmann, T., Kazarian, F., Arambhadiya, B., Bora, D., Jaquinot, J., Mitteau, R., Schuller, F.C., Tanga, A., et al., Proceedings of the 18th Topical Conference on Radio Frequency Power in Plasmas, Ghent, Belgium, AIP Conference Proceedings 1187 (2009) p 265.

60. Lee, D.S., Hong, S., Kim, Kim, K.P., Kim, S.H., Kim, J.S., Wang, S.J., Kim, W.C., Park, K.R., Kwak, J.G. and KSTAR Team, Transactions on Fusion Science and Technology 60 (2011) p. 94.

61. Lerche, E., Van Eester, D., Krasilnikov, A., Ongena, J., Lamalle, P., and JET-EFDA contributors, Plasma Physics and Controlled Fusion 51 (2009) 044006.

62. Lerche, E., Van Eester, D., Johnson, T.J., Hellsten, T., Ongena, J., Mayoral, M.-L., Frigone, D., Sozzi, C., Calabro, G., Lennholm, M., et al., Plasma Physics and Controlled Fusion 54 (2012) 074008.

63. Lin, Y., Binus, A. and Wukitch, S.J., Fusion Engineering and Design 84 (2009) p. 33.

64. Lin, Y., Rice, J.E., Wukitch, S., Reinke, M.L., Greenwald, M.J., Hubbard, A.E., Marmar, E.S., Podpaly, Y., Porkolab, M., Tsujii, N., and the Alcator C-Mod Team, Nuclear Fusion 51 (2011) 063002.

65. Lin, Y., Mantica, P., Hellsten, T., Kiptily, V., Lerche, E., Nave, M.F.F., Rice, J.E., Van Eester, D., de Vries, P.C., Felton, R., et al., Plasma Physics and Controlled Fusion 54 (2012) 074001.

66. Lin, Y., Rice, J.E., Wukitch, S., Greenwald, M.J., Hubbard, A.E., Ince-Cushman, A., Lin, L., Porkolab, M., Reinke, M., and Tsujii, T., Physical Review Letters 101 (2008) 235002.

67. Liu, D., Heidbrink, W.W., Podesta, M., Bell, R.E., Fredrickson, E.D., Medley, S.S., Harvey, R.W., and Ruskov, E., Plasma Physics and Controlled Fusion 52 (2010) 025006.

68. Lennholm, M., Blackman, T., Chapman, I.T., Eriksson, L.-G., Graves, J.P., Howell, D.F., de Baar, M., Calabro, G., Dumont, R., Graham, M., et al., Nuclear Fusion 51 (2011) 0703032.

69. Louche, F. Dumortier, P., Messiaen, M. and Durodie, F. Nuclear Fusion 51 (2011) 103002.

70. Lyssoivan, A. Douai, D., Koch, R., Ongena, J., Phillips, V., Schiller, F.C., Van Eester, D., Wauters, T., Blackman, T., Bobkov, V., et al., Plasma Physics and Controlled Fusion 54 (2012) 074014.

71. Mendes, A., Colas, L., Vulliez, K., Ekedahl, A., Argouarch, A., and Milanesio, D., Nuclear Fusion 50 (2010) 025021.

72. Messiaen, A., Vervier, M., Dumortier, P., Grine, D., Lamalle, P.U., Durodie, F., Koch, R., louche, F., and Weynants, R., Nuclear Fusion 49 (2009) 05504.

73. Messiaen, A., Dumortier, P., Kyrytsya, V., Louche, F., and Vervier, M., Fusion Engineering and Design 86 (2011) 855.

74. Messiaen, A. and Weynants, R. Plasma Physics and Controlled Fusion 53 (2011) 085020.

75. Messiaen, A., Koch, R. Weynants, R.R., Dumortier, P., Louche, F., Maggiora, R. and Milanesio, D., Nuclear Fusion 50 (2010) 025026.

76. Milanesio, D. and Maggiora, R., Nuclear Fusion 50 (2010) 025007.

77. Milanesio, D. Meneghini, O., Lancellotti, V., Maggiora, R. and Vecchi, G., Nuclear Fusion 49 (2009) 115019.

78. Murakami, M., Park, J.M., Giruzzi, G., Garcia, J., Bonoli, P., Budny, R., Doyle, E.J., Fukuyama, A., Hayashi, N., Honda, M., et al., Nuclear Fusion 51 (2011) 103006.

79. Myra, J.R., and D'Ippolito, D.A., Physical Review Letters (2008) 195004.

80. Myra, J.R., and D'Ippolito, D.A., Plasma Physics and Controlled Fusion 52 (2010) 015003.

81. Nordman, H., Singh, R., Futop, T., Eriksson, L.-G., Dumont, R., Anderson, J., Kaw, P., Strand, P., Tokar, M., and Weiland, J., Physics of Plasmas 15 (2008) 042316.

82. Pace, D.C., Pinsker, R.I., Heidbrink, W.W., Fisher, R.K., Van Zeeland, M.A., Austin, M.E., McKee, G.R., and Garcia-Munoz, M., Nuclear Fusion 52 (2012) 063019.

83. Parail, V., Belo, P. Boerner, P., Bonnin, X., Corrigan, G., Coster, D., Ferreira, J., Foster, A., Garzotti, L., Hogewell, G.M.D., et al., Nuclear Fusion 49 (2009) 075030.

84. Parisot, A., Wukitch, S.J., Bonoli, P., Greenwald, M., Hubbard, A., Lin, Y., Parker, R., Porkolab, M., Ram, A.K., and Wright, J., Plasma Physics And Controlled Fusion 49 (2007) p.219.

85. Paul, M.K., Lyssoivan, A., Koch, R., Van Wassenhove, G., Vervier, M., Bertschinger, G., Laengner, R., Unterberg, B., Sergienko, G., Phillips, V., et al., Fusion Engineering and Design 88 (2013) p. 51.

86. Paul, M.K., Lyssoivan, S. Koch, R., Wauters, T., Douai, D., Bobkov, V., Van Eester, D., Lerche, E., Ongena, J., Rohde, V., et al., Fusion Engineering and Design 87 (2012) p. 98.

87. Perkins, F.W., Nuclear Fusion 17 (1977) p. 1197.

88. Perkins, R.J., Hosea, J.C., Kramer, G.J., Ahn, J.W., Bell, R.E., Diallo, A., Gerhardt, S., Gray, T.K., Green, D.L., Jaeger, E.F., et al., Physical Review Letters 109 (2012) 045001.

89. Phillips, C.K., Bell, M., Bell, R.E., Bernabei, S., Fredrickson, E., Hosea, J.C., LeBlanc, B., Majeski, R., Medley, S., Ono, M., et al., Proceedings of the 13th Conference on RF Power in Plasmas Annapolis MD, USA, AIP Conf. Proceedings 485 (1999) p. 69.

90. Poli, F.M. and Kessel. C.E., Physics of Plasmas **20,** 056105 (2013).

91. Prechtl, M., Bobkov, V., Braun, F., Faugel, H., and Noterdaeme, J.-M., Fusion Engineering and Design 84 (2009) p. 1539.

92. Reinke, M.L., Hutchinson, I.H., Rice J.E., Howard, N.T., Bader, A., Wukitch, S., Lin, Y., Pace, D.C., Hubbard, A., Hughes J.W., and Podpaly, Y., Plasma Physics and Controlled Fusion 54 (2012) 043004.

93. Rimini F.G., Andrew, P., Balet, B., Bull, J., Deliyanakis, N., De Esch, H.P.L., Eriksson, L-G., Gormezano, C., Gowers, C.W., Guo, H.Y., et al., Nuclear Fusion 39 (1999) p. 1591.

94. Salvador, S.M., Maggiora, R., D'Inca, R., and Fuenfgelder, H., Proceedings of the 19th Topical Conference on Radio Frequency Power in Plasmas, Newport, Rhode Island, USA, AIP Conference proceedings 1406 (2011) p. 25.

95. Sips, A.C.C., and Gruber, O. Plasma Physics and Controlled Fusion 50 (2008) 124028.

96. Sommer, F., Stober, J., Angioni, C., Bernert, M., Burckhart, A., Bobkov, V., Fischer, R., Fuchs, C., McDermott, R.M., Suttrop, W., Viezzer, E., and the ASDEX Upgrade Team, Nuclear Fusion 52 (2012) 114018.

97. Start, D.F.H., Jacquinot, J., Bergeaud, V., Bhatnager, V.P., Conroy, S.W., Cottrell, G.A., Clement, S., Ericsson, G., Eriksson, L-G., Fasoli, A., et al., Nuclear Fusion 39 (1999) p. 321.

98. Stix, T.H. Nuclear Fusion 15 (1975) p. 737.

99. Tang, V., Parker, R.R., Bonoli, P.T., Wright, J.C., Granetz, R.S., Harvey, R.W., Jaeger, E.F., Liptac, J., Fiore, C.L., Greenwald, M., et al., Plasma Physics and Controlled Fusion 49 (2007) p. 873.

100.   Taylor, G. Hosea, J.C., Kessel, C.E., LeBlanc, B.P., Mueller, D., Phillips, C.K., Valeo, E.J., Wilson, J.R., Ryan, P.M, Bonoli, P.T., Wright, J.C., and Harvey R.W., Physics of Plasmas 19 (2012) 042501.

101.   Tsuji, N., Porkolab, M., Bonoli, P.T., Lin, Y., Wright, J.C., Wukitch, S., Jaeger, E.F., Green, D.L., and Harvey, R.W., Physics of Plasmas 19 (2012) 082508.

102.   Valisa, M., Carraro, L., Predebon, I., Pulatti, M.E., Angioni, C., Coffey, I., Giroud, C., Lauro Taroni, L., Alper, B.,Baruzzo, M., et al., Nuclear Fusion 51 (2011) 033002.

103.   Van Eester, D., Lerche, E., Andrew, Y., Biewer, T.M., Casati, A., Crombe, K., de la Luna, E., Ericsson, G., Felton, R., Giacomelli, L., et al., Plasma Physics and Controlled Fusion 51 (2009) 044007.

104.   Van Eester, D. Lerche, E., Johnson T.J., Hellsten, T., Ongena, J., Mayoral, M.-L., Frigone, D., Sozzi, C., Calabro, G., Lennholm, M., et al., Plasma Physics and Controlled Fusion 54 (2012) 074009.

105.   Van Eester, D., and Lerche, E., Plasma Physics and Controlled Fusion 53 (2011) 092001.

106.   Van Eester, D. Transactions of Fusion Science and Technology 57 (2010) p. 106.

107.   Van Eester, D., Crombe, K., and Kyrytsya, V. Plasma Physics and Controlled Fusion 55 (2013) 025002.

108.   Versloot, T.W., Sartori, R., Rimini, F., de Vries, P.C., Saibene, G., Parail, V., Beurskens, M.N.A., Boboc, A., Budny, R., Crombe K., et al., Nuclear Fusion 51 (2011) 103033.

109.   Vranken, M., Argouarch, A., Blackman, T., Dumortier, P., Durodie, F., Evrard, M., Goulding, R.H., Graham, M., Huygen, S., Jacquet, Ph., et al., Fusion Engineering and Design D 84 (2009) p 1953.

110.   Vrancken, M., Lerche, E., Blackman, T., Durodie, F., Evrard, M., Graham, M., Jaquet, P., Kaye, A., Mayoral, M.-L., Nightingale, M.P.S., et al., Fusion Engineering and Design 86 (2011) p. 522.

111.   Wagner, F., Becoulet, A., Budny, R., Erckmann, V., Farina, D., Giruzzi, G., Kamada, Y., Kaye, A., Koechi, F., Lackner, K., et al., Plasma Physics and Controlled Fusion 52 (2010) 124044.

112.   Waltz, R.E., Plasma Physics 4 (1997) 2482.

113. Wilson, J.R., Bush, C. E., Darrow, D., Hosea, J.C., Jaeger, E.F., Majeski, R., Murakami, M., Phillips, C.K., Rogers, J.H., Schilling, G., et al., Physical Review Letters 75 (1995) p. 842.

114. Wukitch, S., Garret, J., Ochoukov, R., Terry, J.L., Hubbard, A., Labombard, B., Lau, C., Lin, Y., Lipschultz, B., Miller, D., Reinke, M.L., Whyte, D. and Alcator C-Mod Team, Physics of Plasmas 20 (2013) 056117.

115. Petrov, Yu. V., and Harvey, R.W., "Finite Orbit Width Features in the CQL3D Code", 24th IAEA Fusion Energy Conference, San Diego, 2012, Paper TH/P6-02.

116. Yu, Y., Hu, J., Zhao, Y., Gao, X., Li, J., and the EAST Team, Plasma Physics and Controlled Fusion 53 (2011) 015013.

117. Zhang, W.Y., Li, Y.D., Zhang, X.J., Lan, T., Gao, X., Liu, Z/X., Sun, P.J., Zhang, X.D., Li, J., and the HT-7 Team, Plasma Physics and Controlled Fusion 54 (2012) 035005.

118. Zhang, X.J., Zhao, Y.P., Wan, B.N., Gong, X.Z., Lin, Y., Zhang, W.Y., Mao, Y.Z., Qin, C.M., Yuan, S., Deng, X., et al., Nuclear Fusion 52 (2012) 082003.

Figure Captions

Figure 1 Layout of the ITER ICRF system. (Lamalle, P.U., Beaumont, B., Gassmann, T., Kazarian, F., Arambhadiya, B., Bora, D., Jaquinot, J., Mitteau, R., Schuller, F.C., Tanga, A., et al., Proceedings of the 18th Topical Conference on Radio Frequency Power in Plasmas, Ghent, Belgium, AIP Conference Proceedings 1187 (2009) p 265.)

Figure 2 The ITER ICRF Antenna (i) The antenna port plug with the eight triple conductor modules (ii) Rear view of the port plug showing one of the four feed modules. (iii) Cut-away view showing a triple element radiating element and its feed. (Borthwick, A., Agarici, G., Davis, A., Dumortier, P., Durodie, F., Fanthome, J., Hamlyn-Harris, C., Hancock, A.D., Lockley, D., Mitteau, R., et al., Fusion Engineering and Design 84 (2009) p. 493.

Figure 3 Critical elements in the plasma density profile for calculating the coupling of the antenna to propagating waves. (Fig. 3 ICRH antenna coupling physics and optimum plasma edge density profile. Application to ITER A Messiaen and R Weynants Plasma Physics and Controlled Fusion 53 085020 2011 IOP).

Figure 4 The JET ITER Like Antenna and the water load used to measure the antenna impedance matrix. (Durodie, F., Nightingale, M., Argourach, A., Berger-By, G.,

Blackman, T., Caughman, J., Cocilovo, V., Dumortier, P., Edwards, P., Fanthome, J., et al., Fusion Engineering and Design, 84 (2009) p. 279.)

Figure 5 Comparison of the power coupled to an ELMy plasma (i) by the 3 dB system hybrid system installed on antennas A and B and (ii) by the antennas C and D in a conventional configuration. The effect of the ELMs on coupled power is greatly reduced in the hybrid configuration. (Fig. 9 Implementation of load resilient ion cyclotron resonant frequency (ICRF) systems to couple high levels of ICRF power to ELMy H-mode plasmas in JET M. Graham, M-L Mayoral, I Monakov et al. Plasma Physics and Controlled Fusion 54 074011 2012 IOP).

Figure 6 Averaged kinetic profiles from ASDEX-U discharges during phases with half ECRH plus half ICRF compared to those with half ECRH plus half NBI: (a) electron (solid) and ion (dashed) temperatures; (b) electron density; (c) toroidal rotation; (d), (e), (f) same data but at the plasma edge. ("H-mode characterization for dominant ECRH and Comparison to dominant NBI and ICRF heating at ASDEX Upgrade", E. Sommer et al., Nucl. Fusion 52, No. 11, 114018 (2012)).

Figure 7 Evolution of radiated power (Red), neutron rate, plasma stored energy (W_{dia}), central electron temperature (T_0) and central electron density (N_0), together with NBI and ICRH powers for a JET discharge heated at the fundamental ion cyclotron resonance.

(Fig. 3 Fundamental ion cyclotron resonance heating of JET deuterium plasmas A.V. Krasilnikov, D. Van Eester, E;. Lerche et al. Plasma Physics and Controlled Fusion 51 044005 2009 IOP).

Figure 8 Comparison of TOMCAT (a) and TORIC (b) calculation results for the absorption coefficients for a T concentration scan. ("Study of ICRH scenarios for thermal ion heating in JET D-T plasmas", Ye.O. Kazakov et al., Nucl. Fusion 52, No. 9, 094012 (2012)).

Figure 9 The Alcator C-Mod helical field-aligned antenna rotated 10 degrees from horizontal (a); Calculated RF potential, evaluated 0.5 cm inward of the antenna limiters for six different antenna phasings. The dotted lines (red) are for a purely horizontal antenna, the dashed line for the field aligned antenna both using a isotropic dielectric load. The solid line (black) uses a cold plasma model. (Garrett, M.J., Wukitch, S.J., Koert, P., Whyte, D.G. Proceedings of the 19th Topical Conference on Radio Frequency Power in Plasmas, Newport, Rhode Island, USA, AIP Conference Proceedings, 1406 (2011) p. 203.)

Figure 10 Alcator C-Mod comparison of (a) Molybdenum (MoXXXI) radiation, Total radiation P_{rad}, for field aligned and non-field aligned antennas. (b) Plasma potential (measured by GPI) as a function of power for the two antenna types showing no difference. (Wukitch, S., Garret, J., Ochoukov, R., Terry, J.L., Hubbard, A., Labombard,

B., Lau, C., Lin, Y., Lipschultz, B., Miller, D., Reinke, M.L., Whyte, D. and Alcator C-Mod Team, Physics of Plasmas 20 (2013) 056117.

Figure 11 Change in central toroidal rotation velocity, Stored energy and electron temperature for a mode conversion (red) and hydrogen minority (blue) heated plasma in Alcator C-Mod. (Lin, Y., Rice, J.E., Wukitch, S., Greenwald, M.J., Hubbard, A.E., Ince-Cushman, A., Lin, L., Porkolab, M., Reinke, M., and Tsujii, T., Physical Review Letters 101 (2008) 235002. "Copyright (2011) by The American Physical Society."

Figure 12 Sawtooth period for three different discharge conditions on JET: -90^0 phasing low ^{3}He concentration (blue); -90^0 phasing high ^{3}He concentration (black) and $+90^0$ phasing low ^{3}He concentration (red). $P_{rf} = 4.5$ MW. ("Experimental verification of sawtooth control by energetic particles in ion cyclotron resonance heated JET tokamak plasmas", J.P. Graves et al., Nucl. Fusion 50, No. 5, 052002 (2010)).

Figure 13 Experimentally observed characteristics of gas breakdown with JET A2 antennas in a safe manner; drop in antenna rf voltage, rise in loading resistance and rise in H_α signal for two different A2-C (black) and A2-D (red) antennas. Fig 17, Simulation of ITER full-field ICWC scenario in JET: RF physics aspects A. Lyssoivan , D. Douai, R. Koch, et al. Plasma Physics and Controlled Fusion, 54 074014 2012.
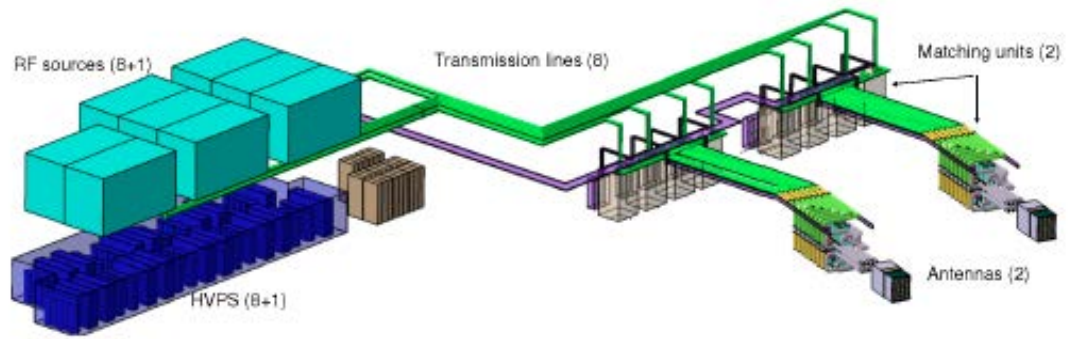
Figure 1
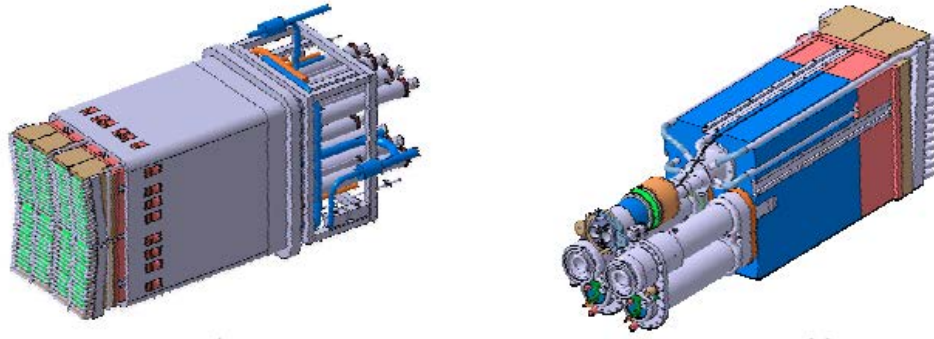
Figure 2 a,b
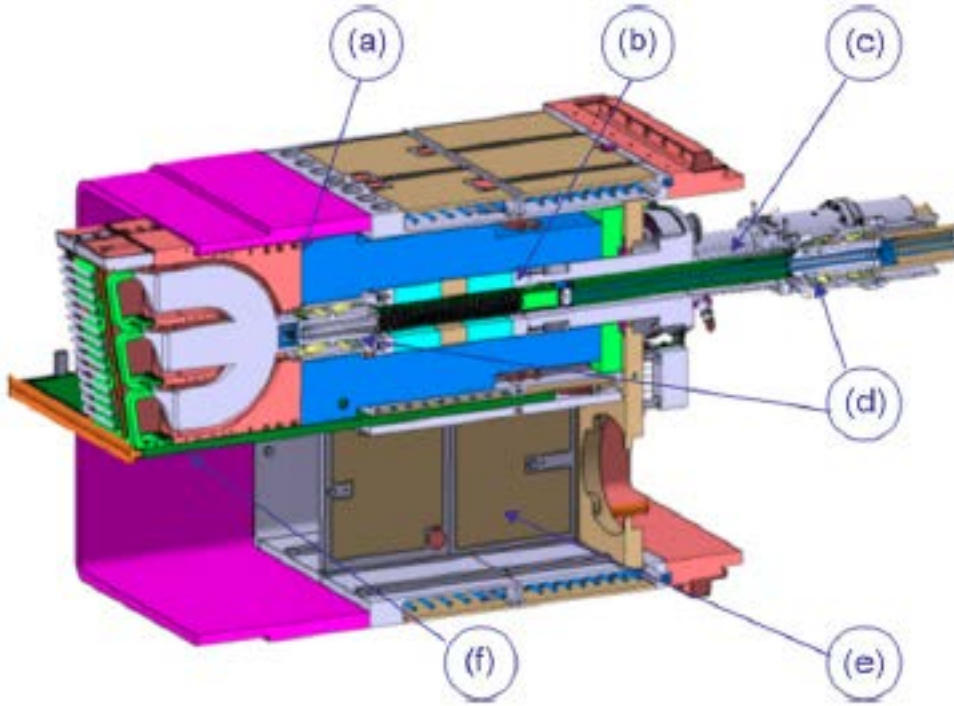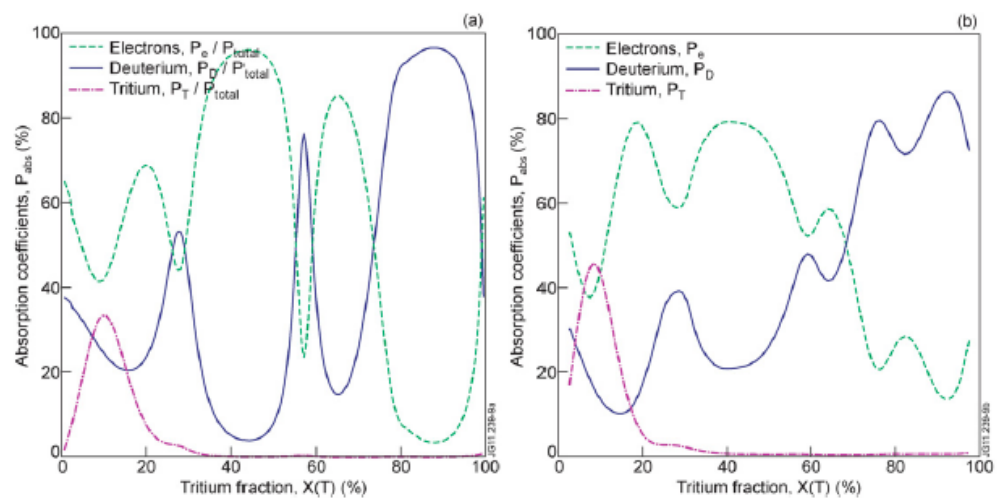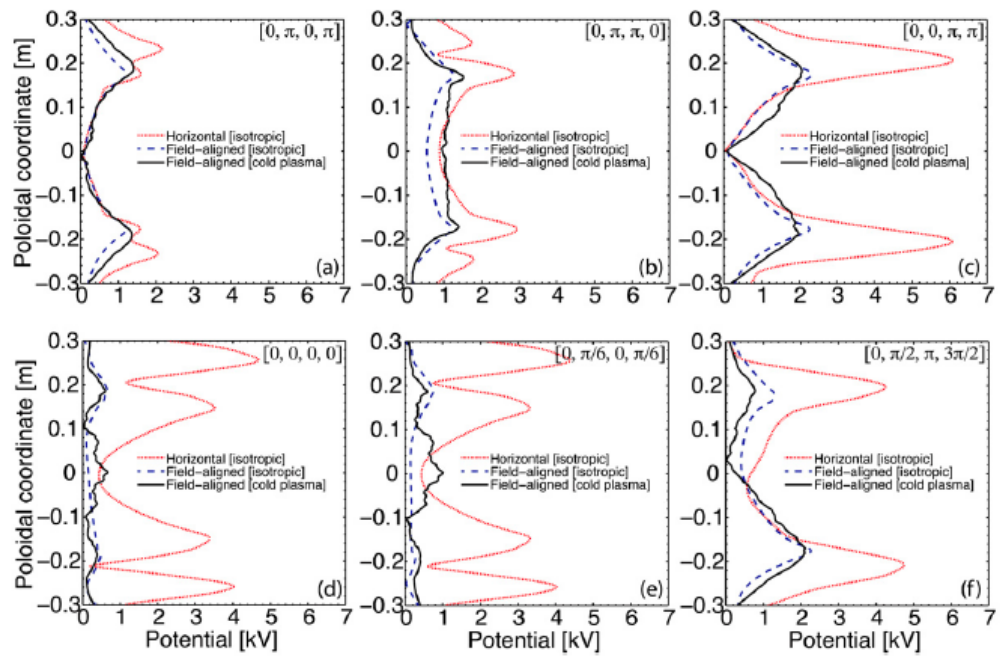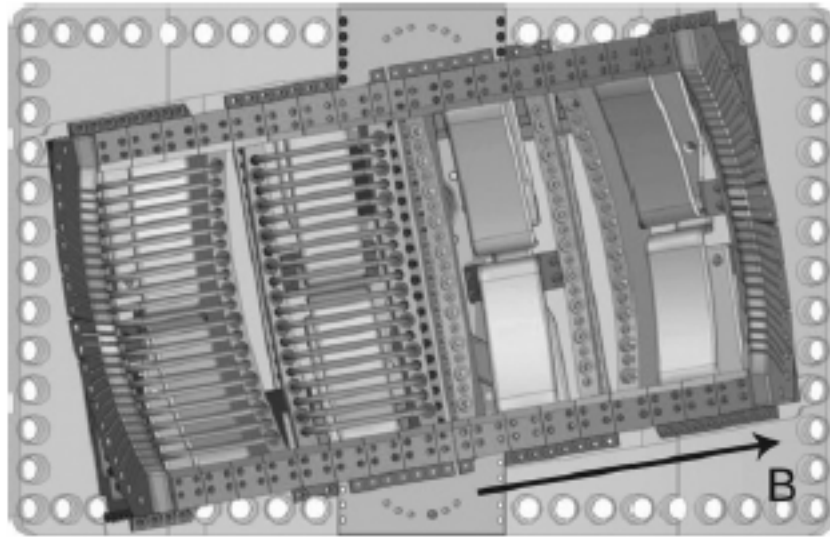
Figure 2 c
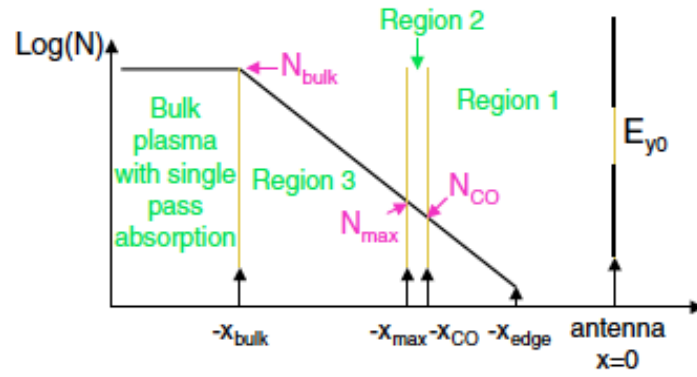
Figure 3

Figure 4
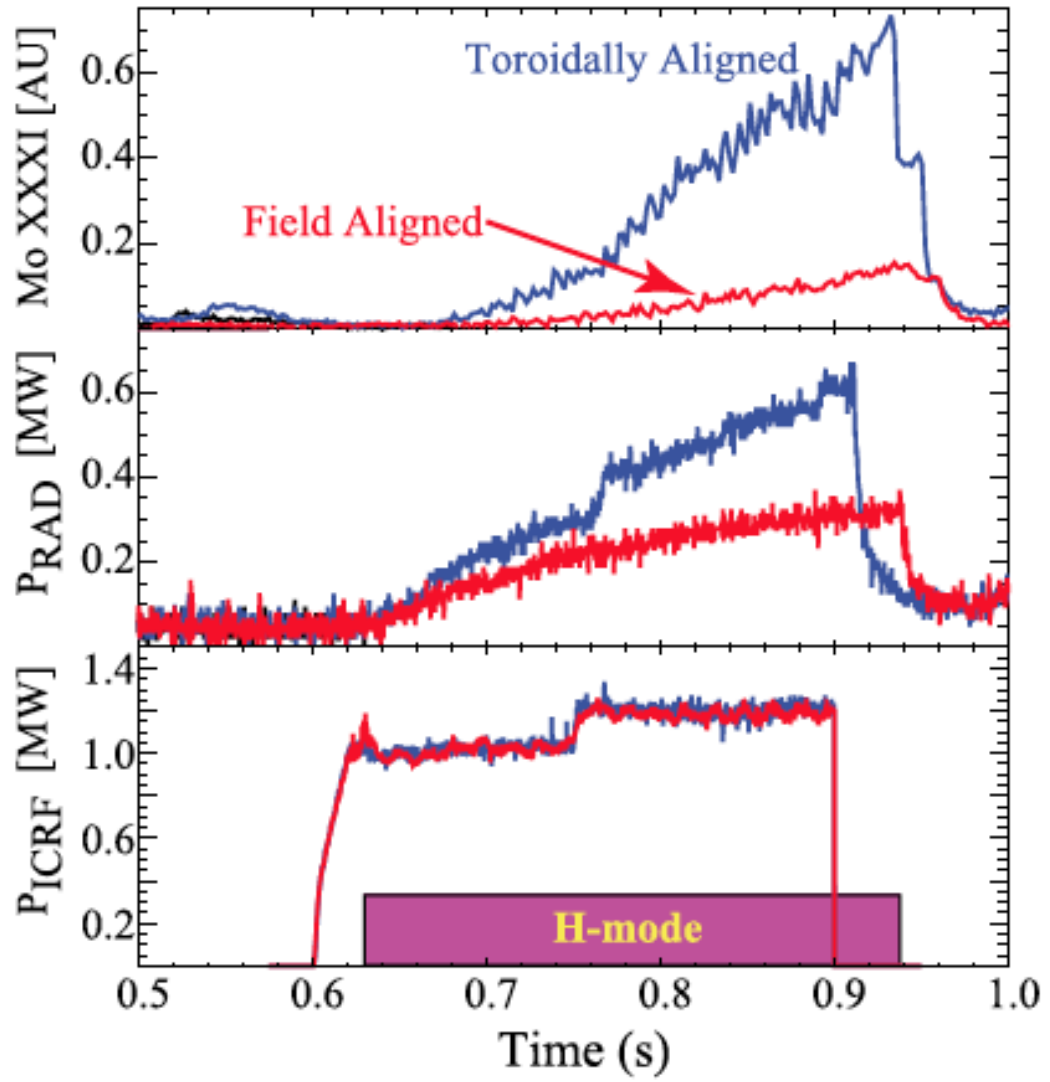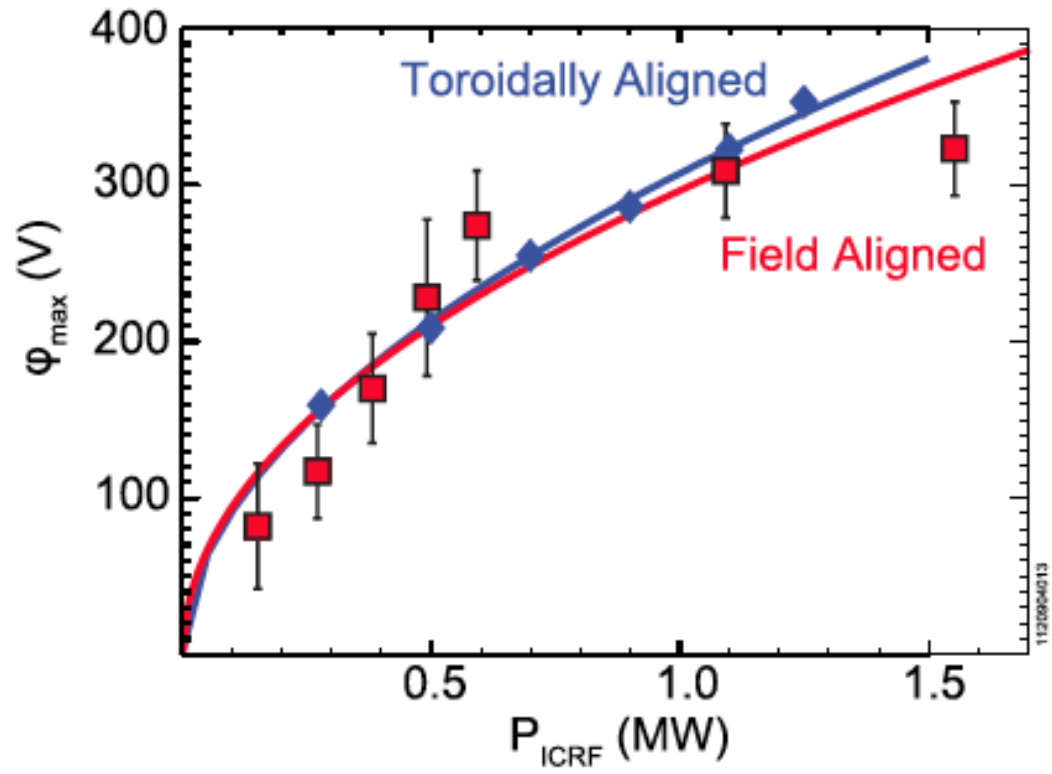
Figure 5

27246,27247

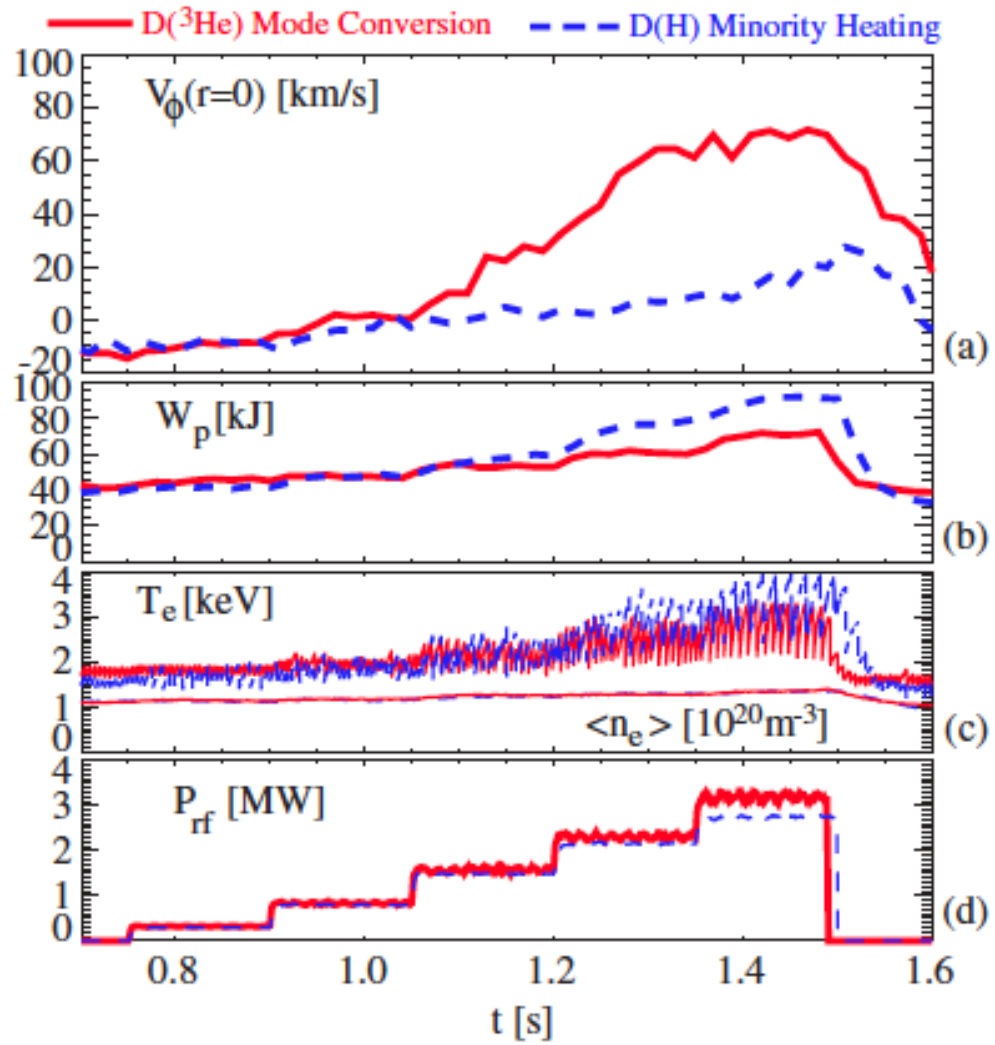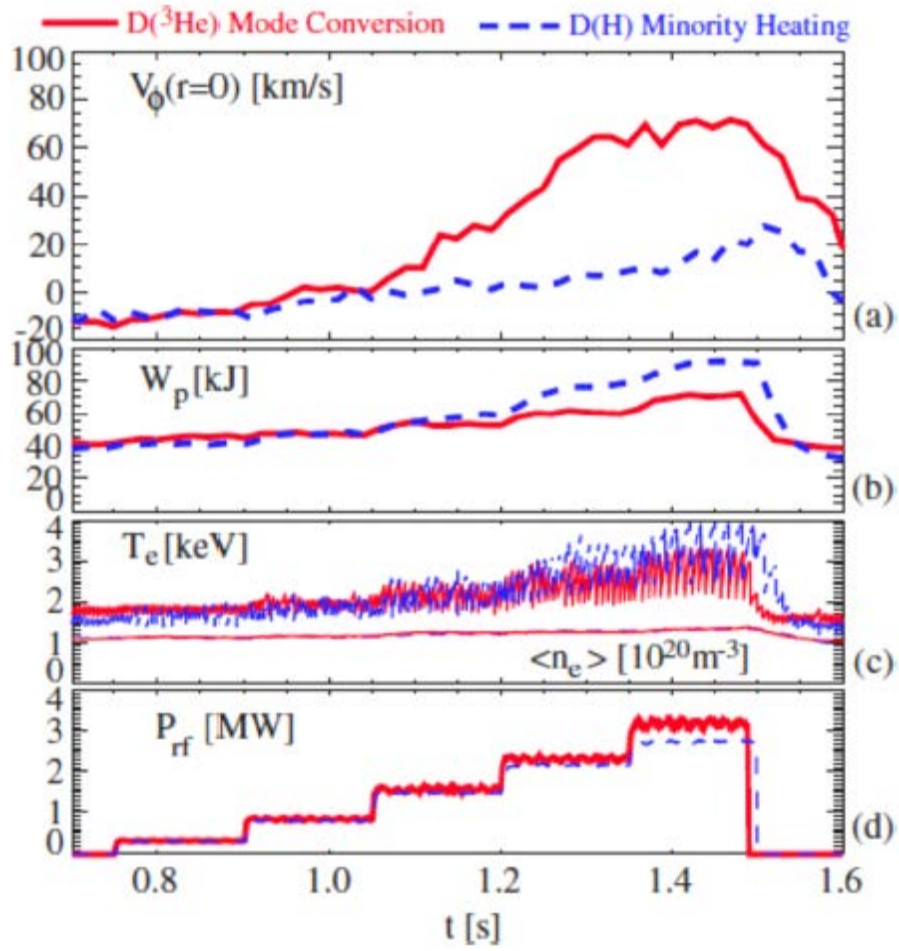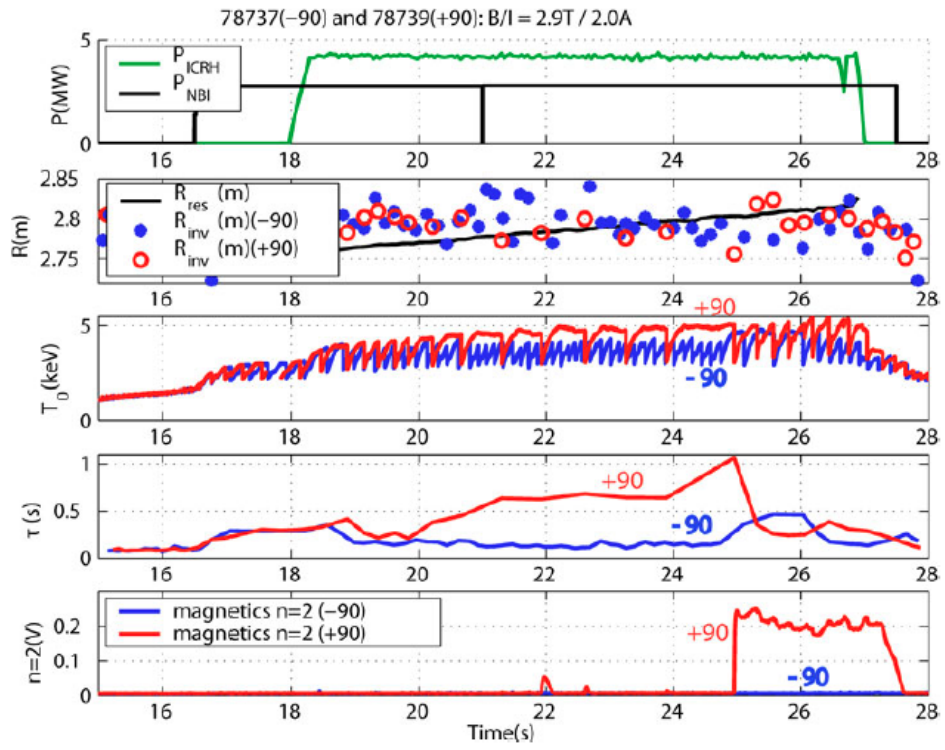Figure 6
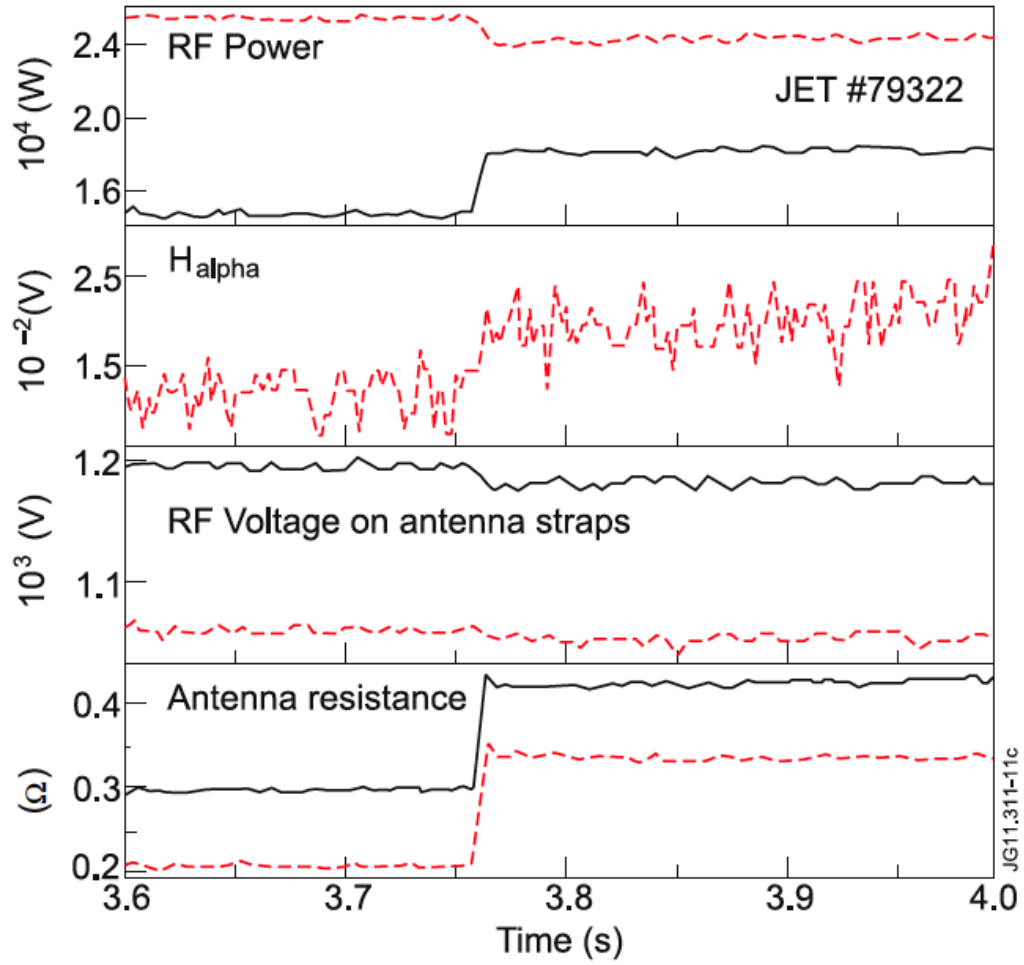
61
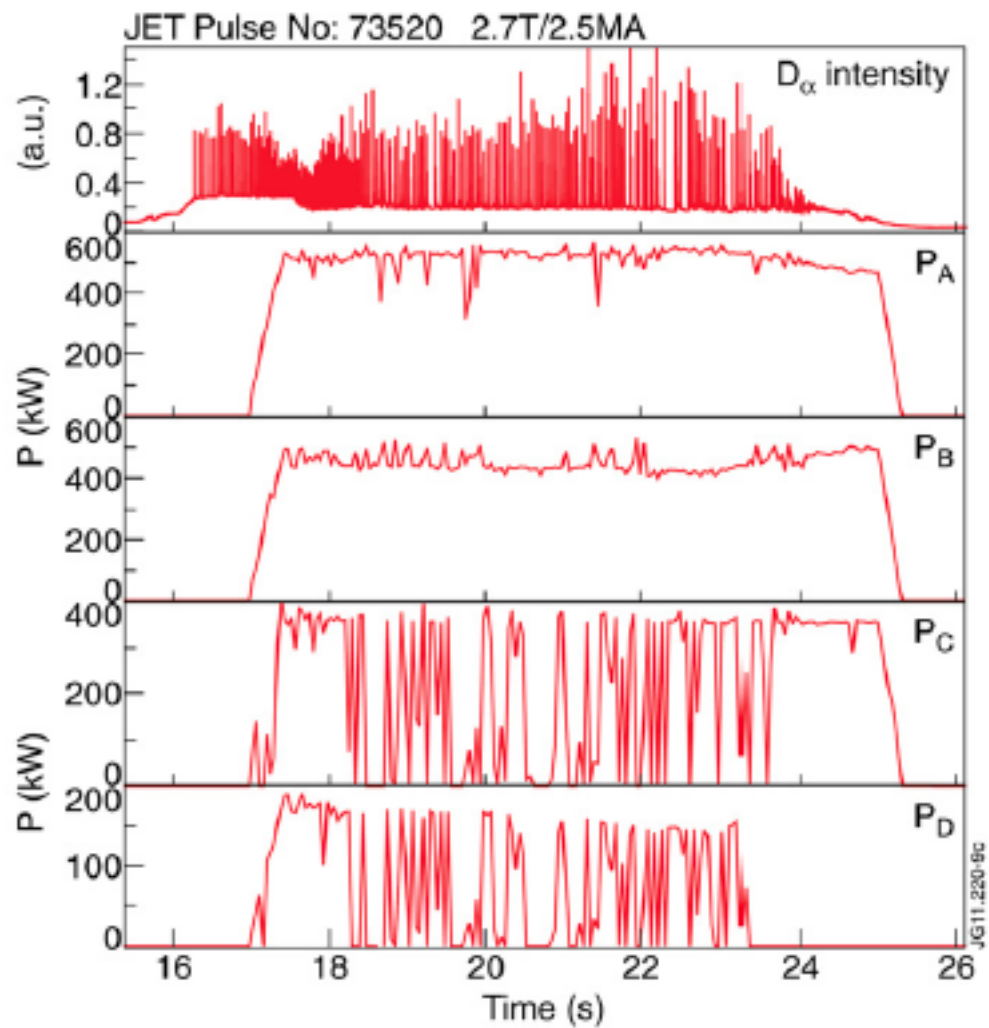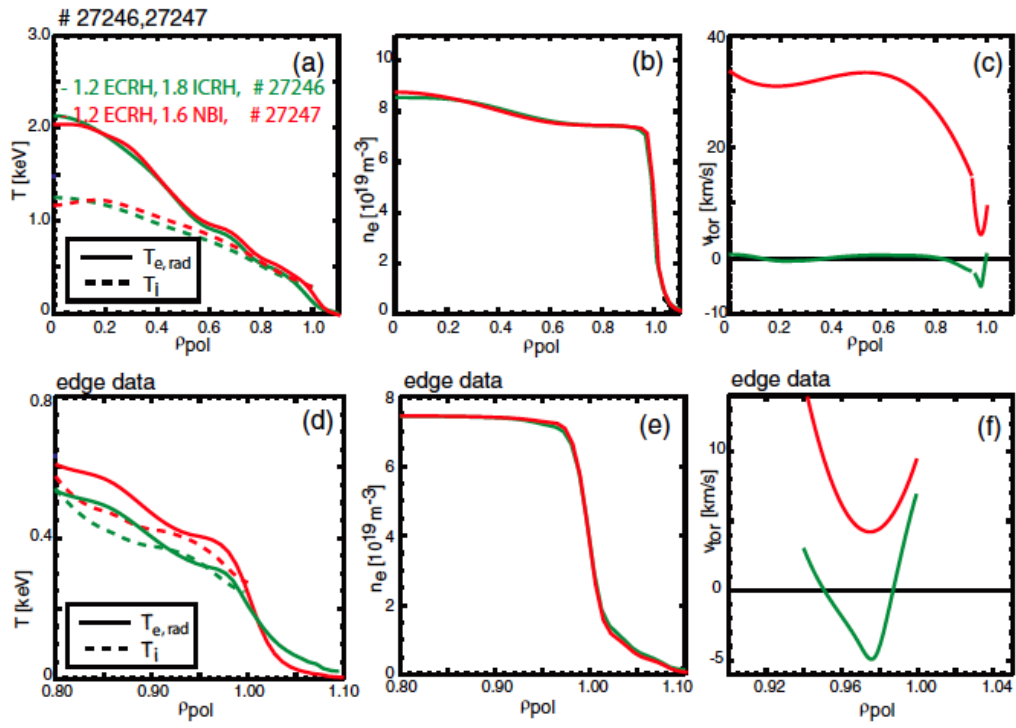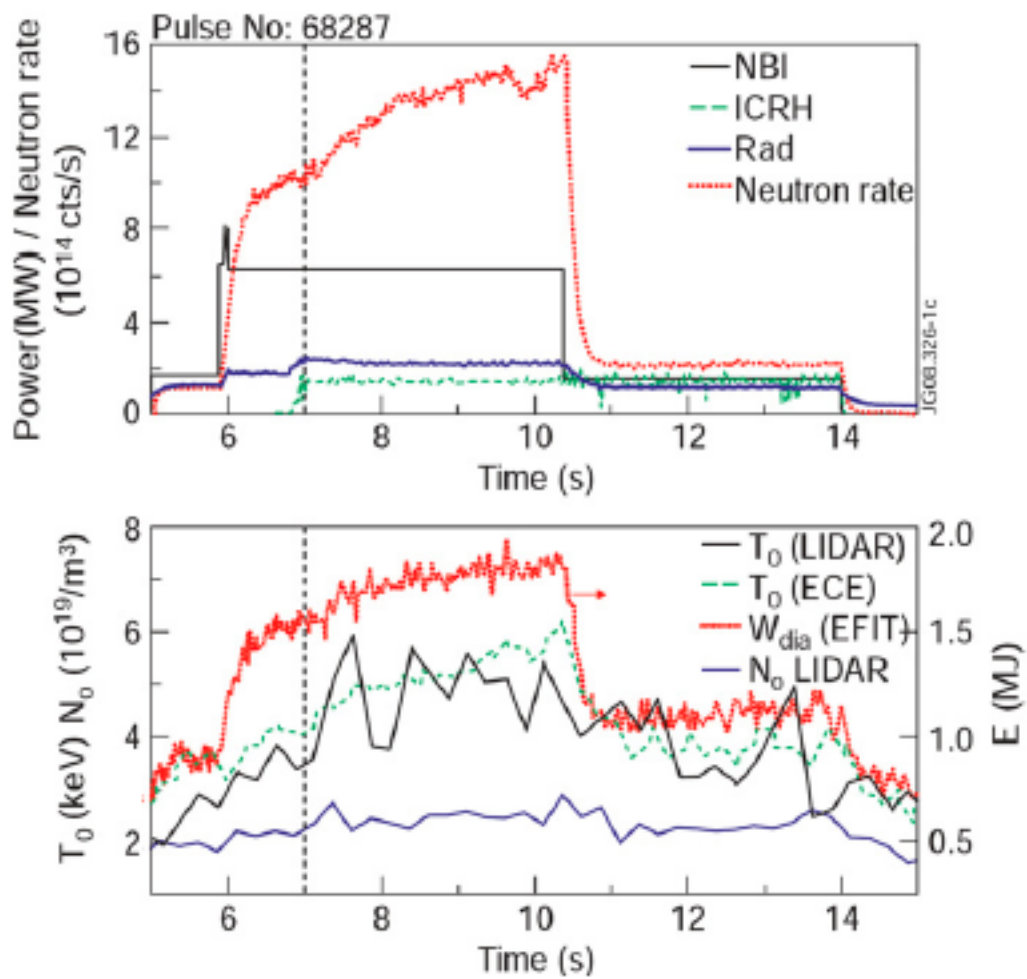
Figure 7

Figure 8

Figure 9

Figure 10 a

Figure 10b

Figure 10c

Figure 11

Figure 12

Figure 13